SANDIA REPORT

SAND98–0567 • UC–705
Unlimited Release
Printed March 1998

Finite-Element/Progressive-Lattice-Sampling Response Surface Methodology and Application to Benchmark Probability Quantification Problems

Vicente J. Romero, Susan D. Bankston

Prepared by
Sandia National Laboratories
Albuquerque, New Mexico 87185 and Livermore, California 94550

Sandia is a multiprogram laboratory operated by Sandia Corporation, a Lockheed Martin Company, for the United States Department of Energy under Contract DE-AC04-94AL85000.

Sandia National Laboratories

Issued by Sandia National Laboratories, operated for the United States Department of Energy by Sandia Corporation.

Available to DOE and DOE contractors from
Office of Scientific and Technical Information
P.O. Box 62
Oak Ridge, TN 37831

Prices available from (615) 576-8401, FTS 626-8401

Available to the public from
National Technical Information Service
U.S. Department of Commerce
5285 Port Royal Rd
Springfield, VA 22161

NTIS price codes
Printed copy: A04
Microfiche copy: A01

SAND98-0567
Unlimited Release
Printed March 1998

Distribution
Category UC-705

Finite-Element/Progressive-Lattice-Sampling Response Surface Methodology and Application to Benchmark Probability Quantification Problems

Vicente J. Romero and Susan D. Bankston
Thermal Sciences Department
Sandia National Laboratories
P.O. Box 5800
Albuquerque, New Mexico 87185-0835

Abstract

Optimal response-surface construction is being investigated as part of Sandia discretionary (LDRD) research into Analytic Nondeterministic Methods. The goal is to achieve an adequate representation of system behavior over the relevant parameter space of a problem with a minimum of computational and user effort. This is important in global optimization and in estimation of system probabilistic response, which are both made more viable by replacing large complex computer models with fast-running accurate and noiseless approximations. A Finite Element / Lattice Sampling (FE/LS) methodology for constructing progressively refined finite element response surfaces that reuse previous generations of samples is described here. Similar finite element implementations can be extended to N-dimensional problems and/or random fields and applied to other types of structured sampling paradigms, such as classical experimental design and Gauss, Lobatto, and Patterson sampling. Here the FE/LS model is applied in a "decoupled" Monte Carlo analysis of two sets of probability quantification test problems. The analytic test problems, spanning a large range of probabilities and very demanding failure-region geometries, constitute a good testbed for comparing the performance of various nondeterministic analysis methods. In results here, FE/LS decoupled Monte Carlo analysis required orders of magnitude less computer time than direct Monte Carlo analysis, with no appreciable loss of accuracy. Thus, when arriving at probabilities or distributions by Monte Carlo, it appears to be more efficient to expend computer-model function evaluations on building a FE/LS response surface than to expend them in direct Monte Carlo sampling.

Table of Contents

1 Introduction

Optimal response-surface construction is being investigated as part of a Laboratory-Directed Research and Development (LDRD) project in Analytic Nondeterministic Methods. The goal is to achieve an adequate representation of system behavior over the relevant parameter space of a problem with a minimum of computational and user effort. This is important in global optimization and in estimation of system probabilistic response, which are both made more viable by replacing large complex computer models of system behavior by fast-running accurate approximations.

Here we report on "progressive Lattice Sampling" in the uncertainty parameter space as a basis for generating successive finite element response surfaces that are increasingly effective in matching actual response functions. Lattice Sampling is only the first of a number of structured sampling arrangements intended for investigation, but already the promise of finite element response surfaces based on structured sampling is evident as will be demonstrated here. Indications are that such response surfaces can be very profitably used in global optimization and nondeterministic analysis as efficient replacements for the full computational models they get their samples from.

One of the strengths of structured global sampling is the ability to prescribe or control the locations of points in the parameter space at which to sample the governing response function (usually represented by a complex finite element model) so as to optimize the global "coverage" of the parameter space when no *a priori* knowledge of the function exists. Successive rounds or levels of sampling can be added for progressive global refinement of the response surface, hopefully making optimal use of previous samples as each new set of samples is added. Structured sampling is innately parallel at each new level and is usually straightforwardly extendable to arbitrary dimensions. With respect to other more global representations such as neural network or wavelet formulations, for a given number of samples, a piecewise-continuous low-order finite element representation usually allows more localized conformance to actual function topology. Furthermore, this representation is conceptually and mathematically simpler, having easily expressible analytic partial derivatives of any order and mixing, which becomes a great advantage in later rounds of analysis during local optimization or adaptive probability estimation. Finally, the representations are unambiguous, having no external free parameters or subjective structural choices as in neural networks and wavelets.

The methodology for constructing piecewise-continuous finite element response surfaces from 2-D Lattice Sampling is presented in Chapter 2 and three supporting Appendices. Building blocks of the methodology can be easily adapted to N-dimensional problems and other sampling schemes. In Chapter 3, progressive FE/LS response surfaces are used in a "decoupled" Monte Carlo procedure to calculate failure probabilities for two sets of very stringent test problems. The efficiencies of decoupled Monte Carlo with FE/LS response surfaces are compared against direct Monte Carlo, and the results indicate that decoupled Monte Carlo is much more efficient. Chapter 4 summarizes the important findings from this work and suggests directions for future research.

2 Finite Element Response Surfaces based on Progressive Global Lattice Sampling

2.1 2-D Formulation

The methodology for constructing globally continuous, piecewise-smooth finite element response surfaces from 2-D Lattice Sampling is presented here.

2.1.1 Finite Element / Lattice Sampling Approximation "Levels"

Figure 2.1 shows unit squares representing an appropriately mapped 2-D parameter space where the mapped parameters both vary between 0 and 1, inclusive. Various discretizations of the parameter space into finite elements are shown. Each discretization level is associated with an increasing number of node or sample points where a test is to be run or a functional evaluation (FEV) of a model is to be performed. The number and location of sample points determine the number and character of finite elements covering the parameter space. Section 2.1.2 and Appendices B and C describe the various finite element types and their structuring into the continuous, piecewise-smooth response surface approximations described and labeled here as Finite Element / Lattice Sampling (FE/LS) "Levels".

Level 1 ◆ A bilinear global approximation function is set up based on four sample points (FEVs of the analytic function) at the four corners of the domain.

Level 2 ● One sample point is added to the center of the parameter space, which is then subdivided into four linear triangles as shown, the associated global response-surface representation being comprised of four linear triangular finite elements supported by the five sample points.

Level 3 ▼ Four sample points are added and the global response surface is reconstituted as one Lagrangian nine-node biquadratic quadrilateral finite element.

Level 4 ■ Four more sample points are added for a total of 13, and the global response surface is rediscretized into one Lagrangian 9-node biquadratic quadrilateral finite element and four linear-to-quadratic transition triangles at the four corners of the domain.

Level 5 ▲ Twelve sample points are added and the global response surface is subdivided into four Lagrangian biquadratic elements supported by a rectangular grid of 25 points.

Level 6 ○ Sixteen sample points are added for a total of 41, and the global response surface is subdivided into four Lagrangian biquadratic quads., four quadratic triangles, and four linear-to-quadratic transition triangles at the four corners of the domain.

The levels are built by adding new sample points to the sample points of the previous levels so that progressive global refinement of the parameter space occurs with a minimum of new samples. Of course, other "Lattice" type schemes are possible, including classical experimental design, which is also presently being investigated. One of the nice features of Lattice-type schemes is that they are conceptually simple and seem to be straightforwardly extendable to arbitrary numbers of dimensions. Other advantages of the approach are elaborated in [1].

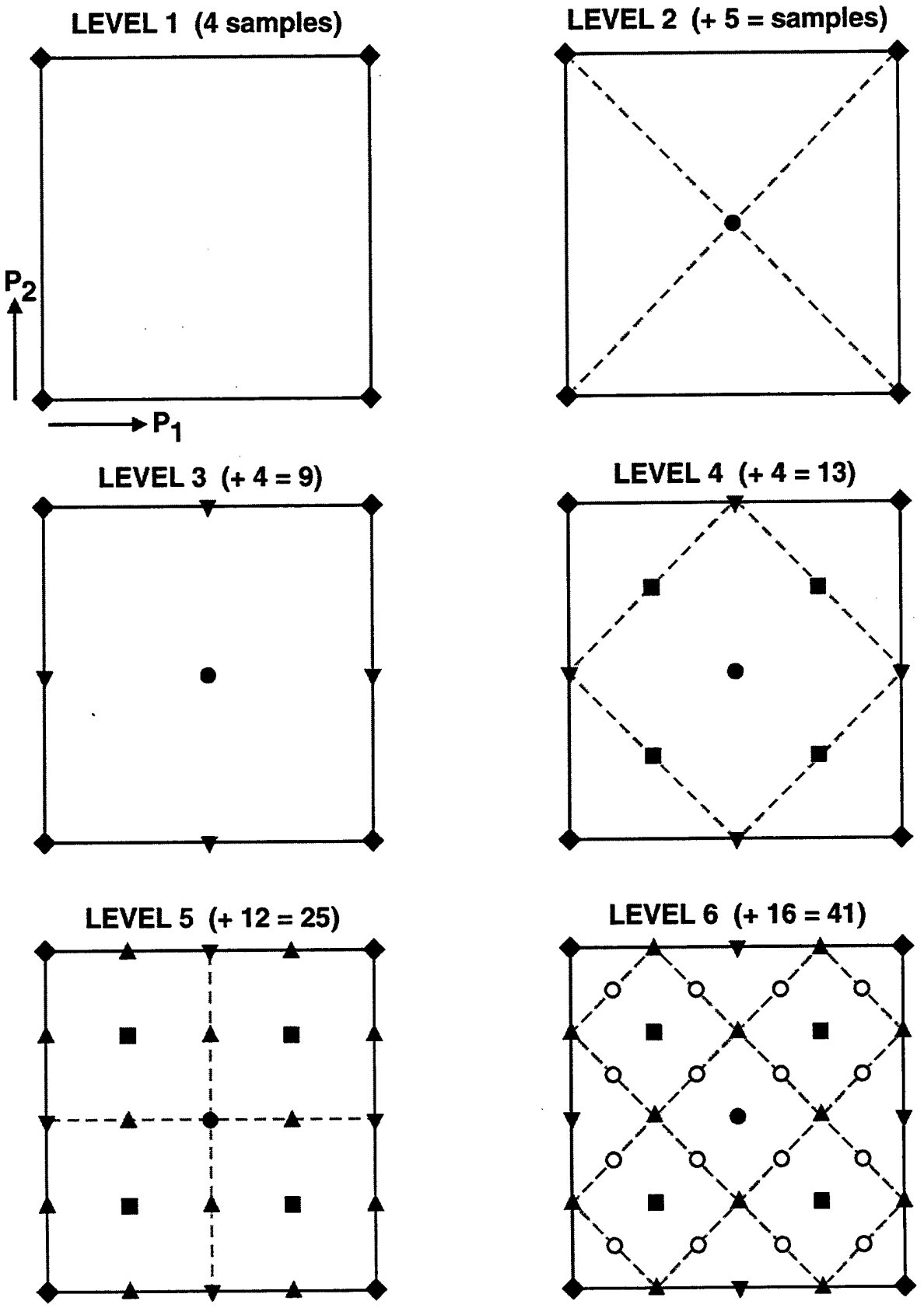

Figure 2.1 2-D Lattice Sampling Levels and associated discretization of the parameter space.

2.1.2 Interpolation Methodology

A FORTRAN77 research code (INTERP1C) was written in this work for generating FE/LS response surfaces corresponding to Levels 1 - 6 and for interpolating off of the response surfaces. Each Level requires the exact values of the "target" function at the associated node points shown in Figure 2.1. These will be referred to as "nodal values". For Level 1 only the exact values at the four corners of the domain must be determined and input to INTERP1C (along with zero values for the other global nodes), whereas for the biquadratic square of Level 3 the nodal values at points numbered 1 - 9 in Figure 2.2 must be calculated, etc. Though the target functions posed in this work are analytic functions, the methodology also applies when the target function is unknown and can only be sampled through experiments or computer runs that would be conducted at the appropriate parameter combinations. The coordinates of the 41 nodes in Figure 2.2 are listed in Table 3.

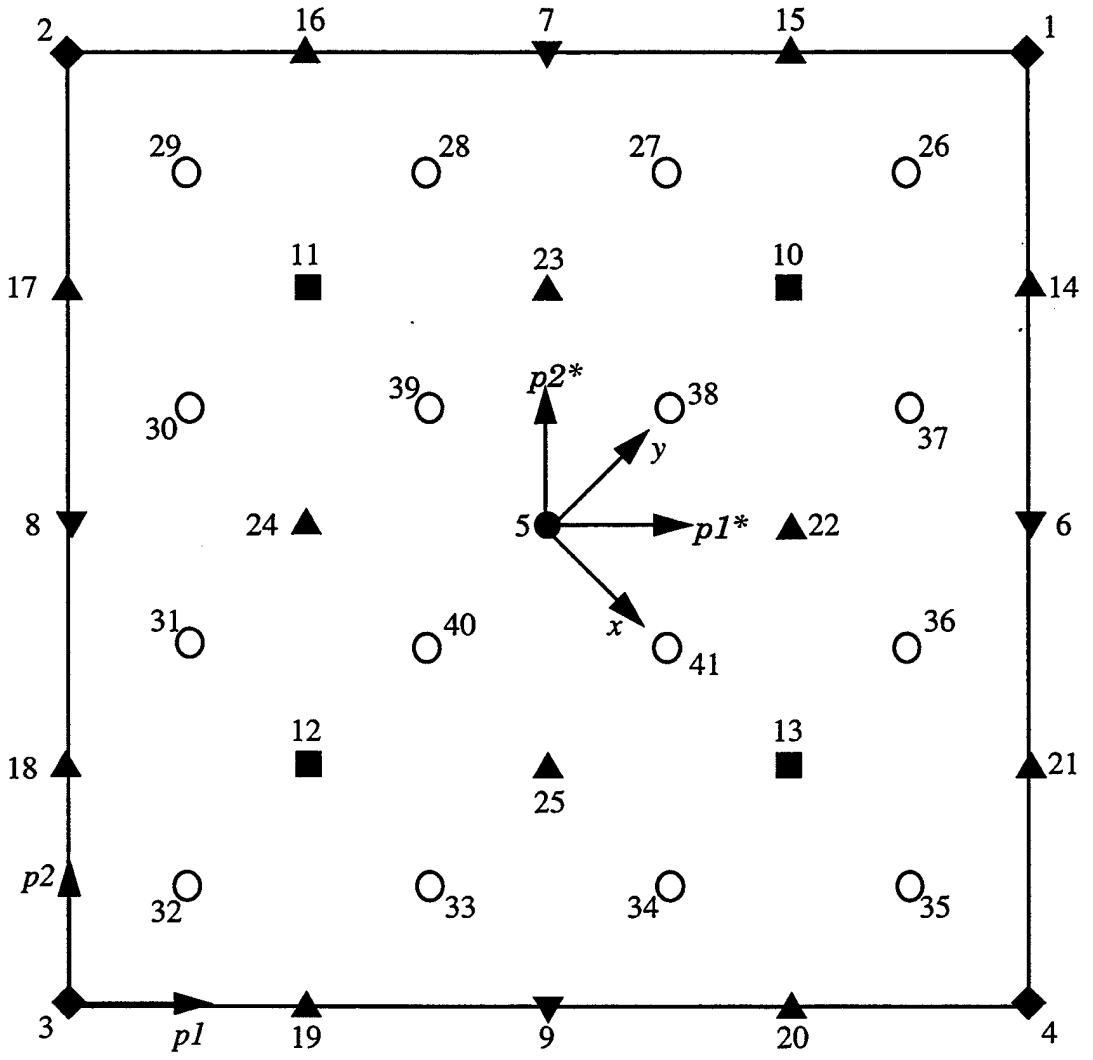

Figure 2.2 Global node numbering scheme for FE/LS response surface Levels 1 - 6.

Table 3 Global coordinates of sampling points in 2-D unit square parameter space

Node number	P1 coordinate	P2 coordinate
1	1.0	1.0
2	0.0	1.0
3	0.0	0.0
4	1.0	0.0
5	0.5	0.5
6	1.0	0.5
7	0.5	1.0
8	0.0	0.5
9	0.5	0.0
10	0.75	0.75
11	0.25	0.75
12	0.25	0.25
13	0.75	0.25
14	1.0	0.75
15	0.75	1.0
16	0.25	1.0
17	0.0	0.75
18	0.0	0.25
19	0.25	0.0
20	0.75	0.0
21	1.0	0.25
22	0.75	0.5
23	0.5	0.75
24	0.25	0.5
25	0.5	0.25
26	0.875	0.875
27	0.625	0.875

Table 3 Global coordinates of sampling points in 2-D unit square parameter space

Node number	P1 coordinate	P2 coordinate
28	0.375	0.875
29	0.125	0.875
30	0.125	0.625
31	0.125	0.375
32	0.125	0.125
33	0.375	0.125
34	0.625	0.125
35	0.875	0.125
36	0.875	0.375
37	0.875	0.625
38	0.625	0.625
39	0.375	0.625
40	0.375	0.375
41	0.625	0.375

With the exact values of the target function known at the appropriate nodal locations specific to a given Level, INTERP1C calculates the interpolated value of the response for any point **P** on the (*p1, p2*) coordinate plane (where both coordinates range from 0 to 1). The origin of the coordinates is on the bottom-left corner of the unit square as shown in Figure 2.2.

First, the global (*p1, p2*) coordinates are transformed using relations in Appendix A to similarly oriented (*p1*, p2**) or to diagonally oriented[1] (*x,y*) coordinates depending on the approximation Level involved. For Levels 1, 3, and 5, the transformation is into (*p1*, p2**) coordinates, and for Levels 2, 4, and 6, the transformation is into (*x,y*) coordinates. Figure 2.2 shows the axes of the transformed coordinate systems. The origins of both systems are at the center of the parameter space, and both are scaled at 1/2 the original scale. Taking the (*p1*, p2**) coordinates for example, the top right edge of the parameter square is at (1,1), and the bottom left edge is at (-1,-1).

The next step is to determine which finite element contains the point **P** for the approximation Level under consideration. For Levels 2, 4, and 6, the diagonal orientation of the (*x,y*) coordinates is the most convenient orientation for making this determination. The logic charts in Appendix B describe the selection algorithm.

1. *i.e.*, rotated clockwise by 45 degrees (θ = - 45 degrees in the coordinate transforms described in Appendix A)

Once the "containing" finite element is identified, a coordinate transformation is made from global ($p1^*$, $p2^*$) or (x,y) coordinates of **P** to local coordinates intrinsic to the finite element. The intrinsic coordinate systems for the various types of finite elements used in this work (see Section 2.1.1) are described in Appendix C. For triangular finite elements the transform relations are also presented in Appendix C. For quadrilateral finite elements the transform relations in Appendix A are used where: rotational offsets of local finite-element coordinate systems relative to the applicable ($p1^*$, $p2^*$) or (x,y) global coordinate system are zero; translational offsets are as depicted in Figures B.1 and B.2 of Appendix B; and the local scaling of intrinsic coordinates is such that they range from -1 to 1 over the element.

Once the intrinsic coordinates of the point **P** within the finite element are determined, a mapping of global nodal values to corresponding local nodes of the finite element takes place and these values are combined according to relations listed in Appendix C to determine the interpolated value of the target function at **P**. The relations are based on standard finite element theory as described in Appendix C, where local finite element node numbering conventions and applicable finite element basis functions are also catalogued.

2.2 Application to Benchmark Test Functions 1 and 2

2.2.1 Test Function 1 (multimodal) and Successive FE/LS Approximations

In the context of reliability or failure probability problems, a multimodal function of the random or uncertain variables might arise, for example, in an application involving relative times of failure of system components that either catalyze or retard potentially catastrophic events in a nuclear power plant. Figure 2.3 shows various representations of an analytic multimodal surface defined by the equation

$$response(p1, p2) = \left[0.8r + 0.35sin\left(2.4\pi\frac{r}{\sqrt{2}}\right)\right][1.5sin(1.3\theta)] \qquad \text{EQ 1}$$

on the domain $0 \le p1, p2 \le 1$, where $r = \sqrt{(p1)^2 + (p2)^2}$, $\theta = atan\left(\frac{p2}{p1}\right)$.

Figure 2.3 shows a plot of the analytic function along with representations corresponding to the six Levels of parameter space resolution depicted in Figure 2.1. The plots are drawn from point-to-point linear interpolation off of a 21 x 21 grid of samples evaluated with the various finite element approximations. Calculating a response distribution from this response function and probability distributions for the variables $p1$ and $p2$ cannot be efficiently accomplished with reliability-based techniques because of the multimodality of the function. However, it makes a good test problem for decoupled and direct Monte Carlo sampling, as demonstrated in Chapter 3. After about Level 5 the finite element approximations appear to match the topology of the exact surface very well. Thus, the "convergence rate" vs. number of analytic function evaluations would appear to be fairly high even for this highly varying surface. A quantitative assessment of convergence rate is made in Chapt. 3. In using the response surface in nondeterministic analysis or global optimization, it would seem to make sense to switch from further global refinement to more localized refinement after about Level 6 so that probabilities or local optima could be more efficiently converged to with any further sampling.

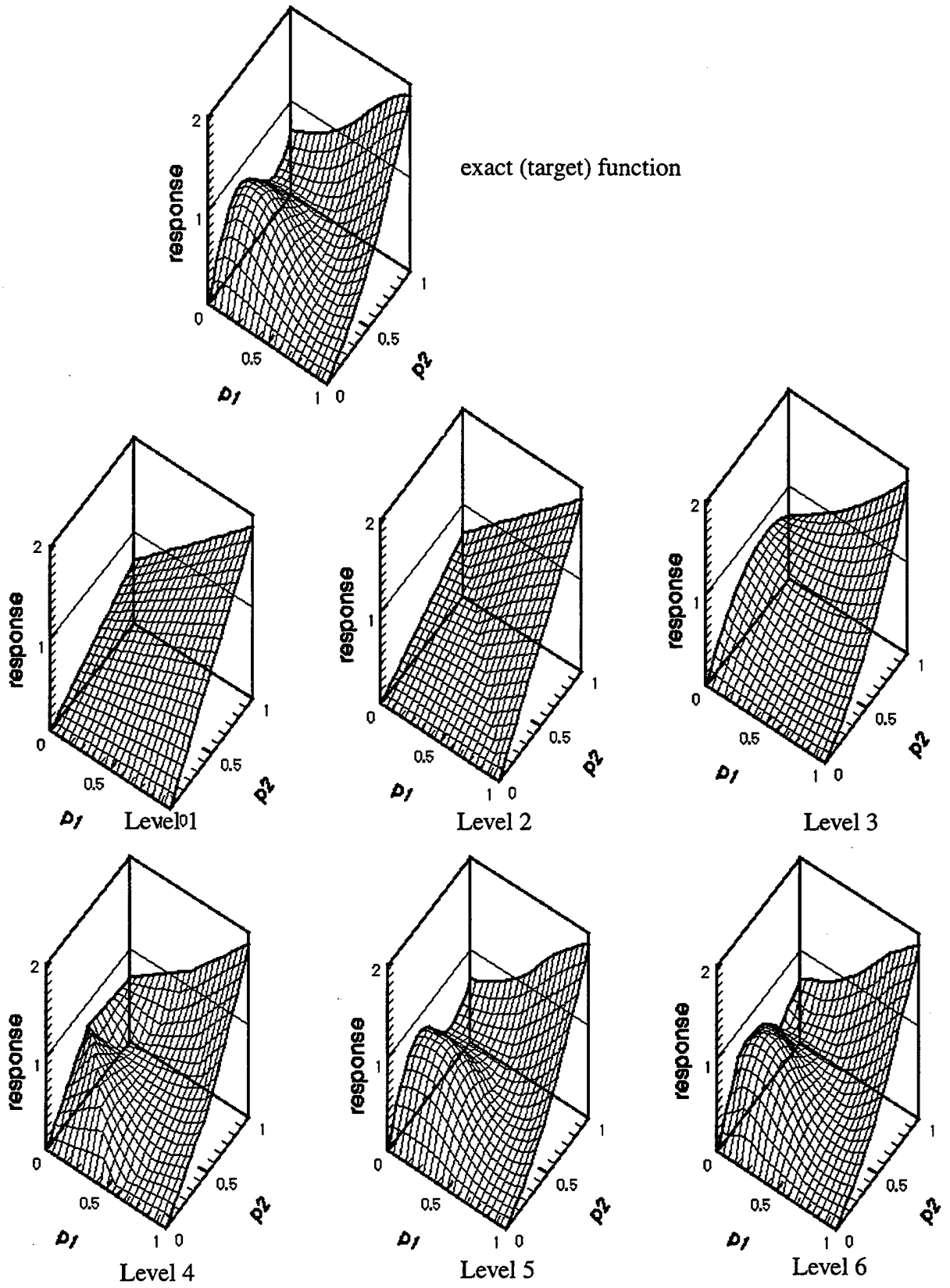

Figure 2.3 Various Lattice Sampling / Finite Element approximation levels, Fcn. 1.

2.2.2 Test Function 2 (monotonic) and Successive FE/LS Approximations

Function 2 is a lower octant of a sphere of radius 1.5 with its center one radius above the origin of the *p1-p2* random-variable coordinate system on which our problem is posed. Figure 2.4 shows various representations of the function corresponding to the six levels of parameter space resolution in the Finite Element / Lattice Sampling (FE/LS) scheme (described in [1]), as well as a representation corresponding to the analytic function itself:

$$response(p1, p2) = 1.5 - \sqrt{(1.5)^2 - r^2} \quad \text{on the domain } 0 \le p1, p2 \le 1 \qquad \text{(EQ 2)}$$

where $r = \sqrt{(p1)^2 + (p2)^2}$. The plots are drawn from point-to-point linear interpolation off of a 21 x 21 grid of samples evaluated with the analytic function or various finite element approximations. A radius of 1.5, which is slightly longer than a diagonal of the *p1-p2* unit square parameter space, was chosen so that the function rises quickly in the further reaches of the parameter space but retains a reasonable slope. Function 2 is representative of many realistic applications in reliability and failure probability assessment where system response is increasingly amplified as the governing parameters increase, such as might occur for structural failure with respect to increasing wind velocity. By Level 3 (nine sample points) the FE/LS representation of the function appears very close. Certainly, the Level 5 representation based on 25 sample points is essentially indistinguishable from the exact function.

2.2.3 Observations

For both Functions the Level 5 approximations based on 25 samples appear to approximate the exact analytic surfaces very well. Therefore, running any nondeterministic analysis method off of the Level 5 response surfaces would seem to yield essentially the same results as running the method off the exact Functions themselves. In fact, when a complex finite element model is used as the "exact" function, running derivative-based optimization and reliability methods off the model might actually be worse than running off an appropriate FE/LS representation because of stochastic numerical noise associated with large mechanics simulations (see - e.g., [2]). This is because numerical derivatives formed with the computational model are generally associated with smaller perturbations of the independent variable(s) than FE/LS representations are, and are therefore more sensitive to perturbations (noise) in the dependent variable.

In the next chapter we will assess the accuracy of the finite element response surfaces in Figure 2.3 and Figure 2.4 with respect to various levels of failure probability calculated from them.

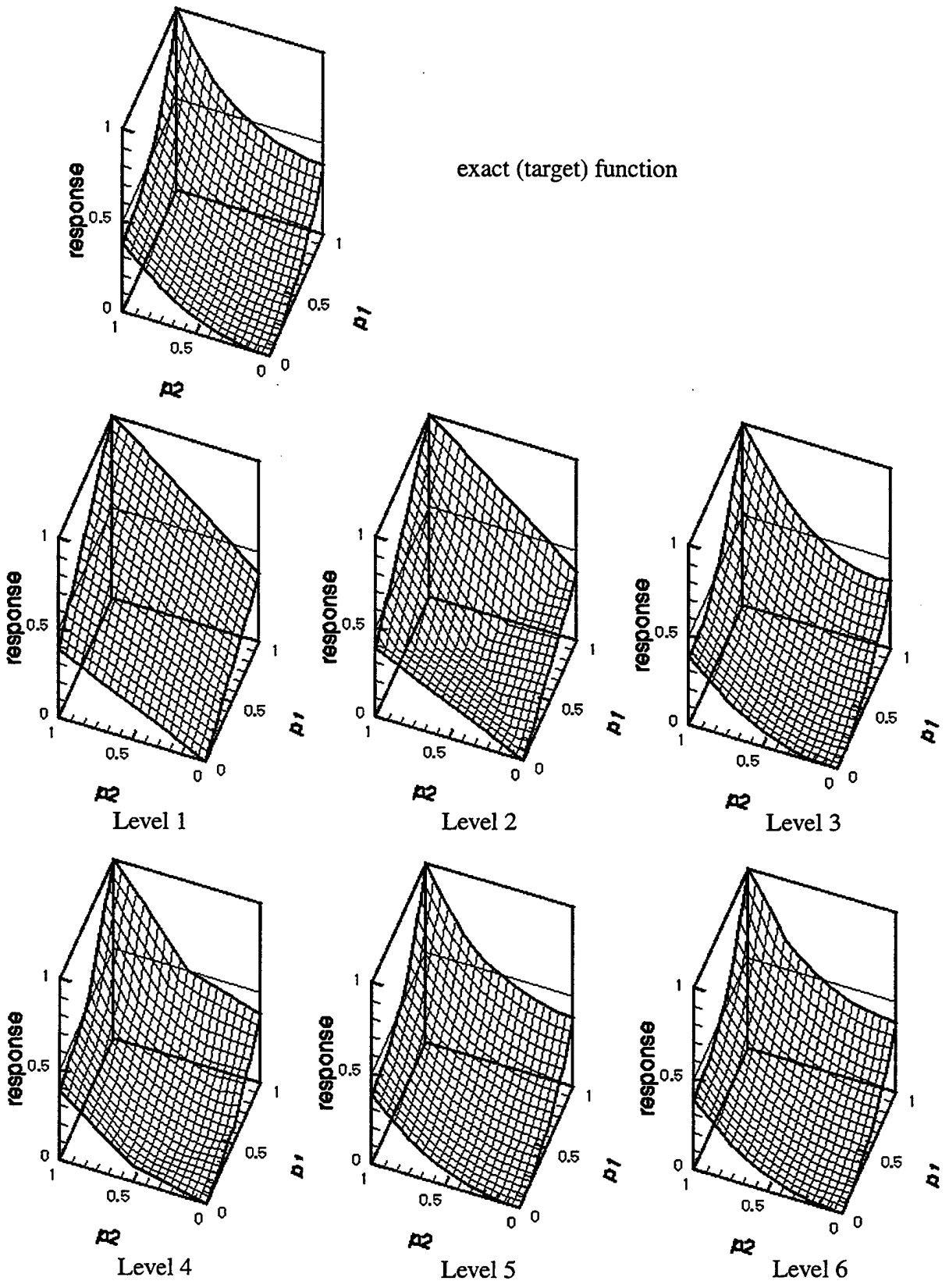

Figure 2.4 Various Lattice Sampling / Finite Element approximation levels, Fcn 2.

3 Performance of Finite Element / Lattice Sampling Response Surfaces on Benchmark Nondeterministic Problems

Here we examine the effectiveness of progressively refined Finite Element / Lattice Sampling (FE/LS) response surfaces in the context of Monte Carlo probability estimation. "Decoupled" Latin Hypercube[5] Monte Carlo sampling uses FE/LS approximations, whereas "direct" Monte Carlo sampling uses the actual function itself. For all problems tested here, decoupled Monte Carlo analysis uses computer model function evaluations more efficiently (generally orders of magnitude more efficiently) than direct Monte Carlo analysis does.

3.1 Description of Joint Probability Density Function

The joint probability density function (JPDF) used in the following study is depicted in Figure 3.1. It is a truncated 2-D standard-normal JPDF of independent normally distributed uncertain parameters *p1* and *p2* with means 0.5 and truncation limits 0 and 1. The standard deviations σ are set such that truncation of the individual distributions occurs at $\pm 3\sigma$ –*i.e.* $\sigma = 0.5/3$– so that the effect of truncation is relatively small.

In Monte Carlo (MC) probability quantification, the prediction of physical response of deterministic (nonstochastic) systems can be decoupled from probabilistic Monte Carlo sampling via intermediate "surrogate" models, such as the FE/LS global response-surface models in Figure 2.2, that often run orders of magnitude faster than full computational physics models. Such an approach is here coined a "decoupled" Monte Carlo approach because the Monte Carlo analysis is decoupled from the running of the full computer model through use of the surrogate model. Because of the numerical noise associated with complex physics simulations (see - *e.g.*, [3] and [4]), surrogate models can also be much more effective in reliability-based approaches to nondeterministic analysis if they meet certain differentiability (smoothness) criteria that can make the optimization process in these approaches more affordable.

Figure 3.2 shows convergence behavior for means and standard deviations for *p1* and *p2* populations ranging from 10^2 to 10^6 samples as generated by the LHS[5] code. The means of both parameters appear to converge to their terminal values within about 100 samples, while the standard deviations stabilize within 1000 samples. (We found that double precision had to be used in our SUN SPARCstation10 LHS computations in order to establish convergence, as the single-precision results showed a suspicious divergent character for population sizes 10^5 and greater.) The population sizes used here extend to 10^6 because it was found that many of the probabilities in the following converged much more slowly than the mean and standard deviations. Presently the convergence rates of moments and probabilities are being explored in connection with automated convergence assessment, incremental sampling, and adaptive termination of Monte Carlo sampling.

3.2 Failure Probability Calculation Method

In the following, failure probabilities are calculated by evaluating a particular exact or approximate response surface shown in Figure 2.3 and Figure 2.4 at all ($p1$, $p2$) parameter sets

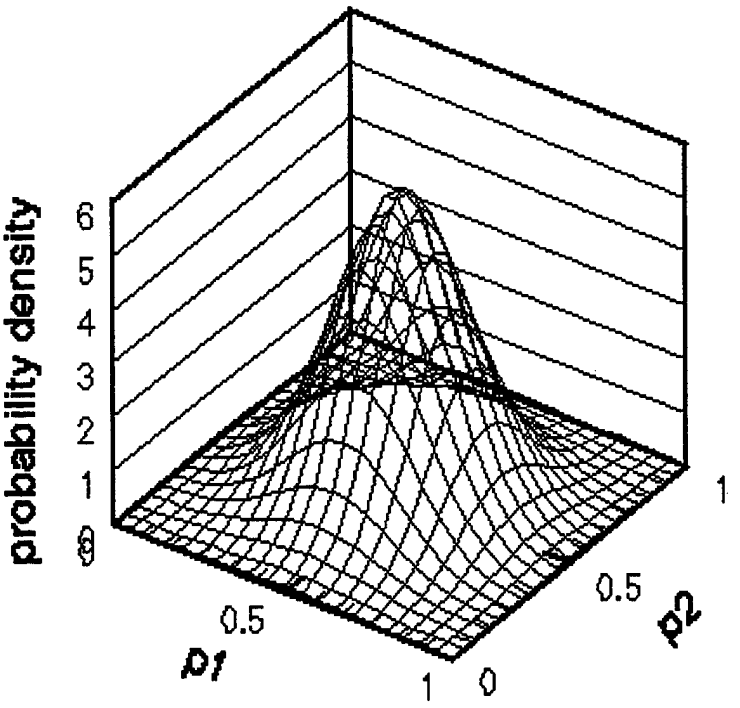

Figure 3.1 Joint Probability Density Function describing the random variables in the problem: normally distributed parameters *p1* and *p2* with means 0.5, std. deviations 0.167, and trunctation of the unit square parameter space at 3σ above and below the means.

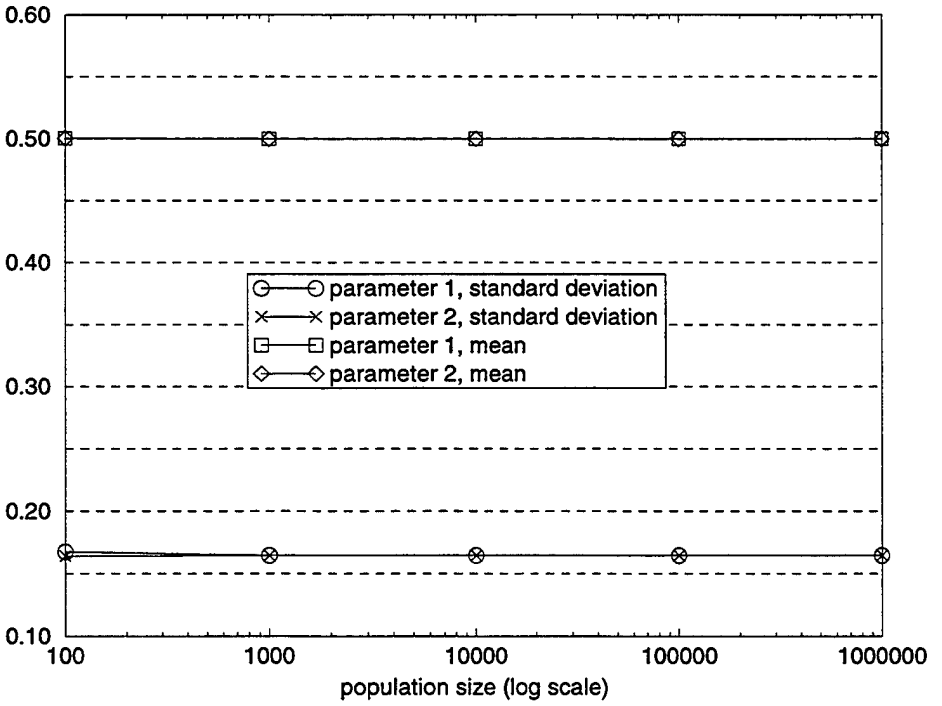

Figure 3.2 Convergence behavior of means and standard deviations of LHS-generated populations from the above JPDF for 100 to 1,000,000 samples in decades.

in a given population of Latin Hypercube samples. The resulting response values are then examined to determine the number of responses in the population at or above a particular threshold value. This number is then divided by the total number of samples in the population to arrive at a failure probability for the given response surface, threshold level, and population size.

3.3 Benchmark Problems

Probabilities are calculated for the following benchmark problems by direct and "decoupled" Latin Hypercube Monte Carlo Sampling according to the JPDF defined above. In the following the shaded regions of the parameter space signify parameter combinations where response exceeds the applicable threshold level. This threshold can be viewed as a failure threshold above which the system response (say that the response metric is shear stress) indicates potential failure of the system. The shaded regions, therefore, denote "failure regions" in the parameter space.

The test functions and response thresholds prescribed here are particularly "good" because they test a large and diverse set of attributes of both Monte Carlo sampling and Lattice sampling. The following benchmark problems encompass a large range of probabilities, on the orders 1 to 10^{-4}. Thus, a large portion of the parameter space is being investigated in this regard.

3.3.1 Function 1, Threshold = 0.2

The shaded regions below signify the parameter space "failure regions" for various representations of Function 1 and a threshold value of 0.2.

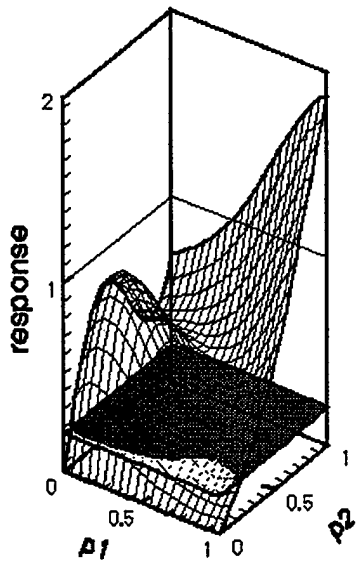

Exact Function cut by threshold plane of response = 0.2

Exact failure region (shaded).

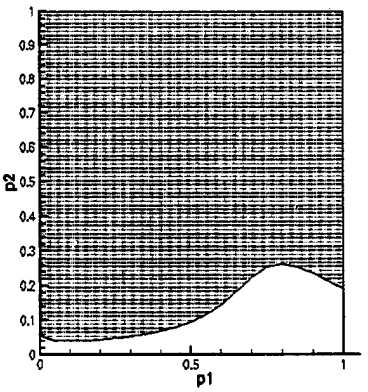

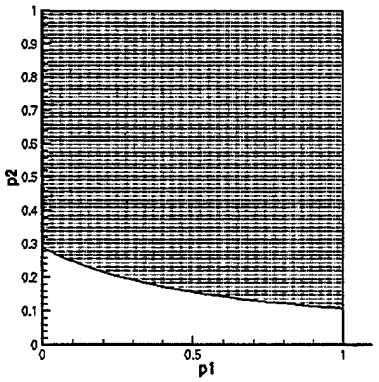

Level 1

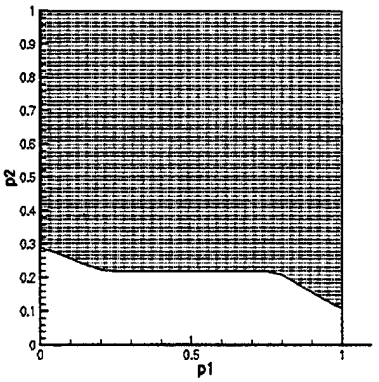

Level 2

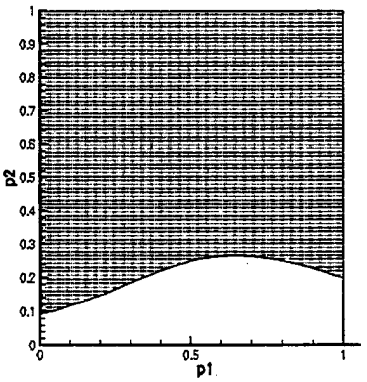

Level 3

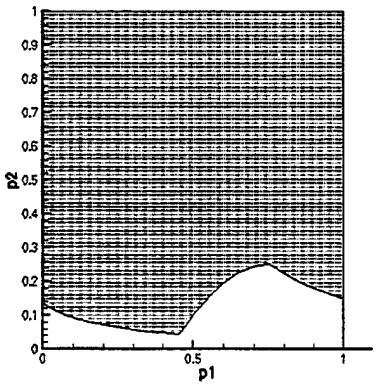

Level 4

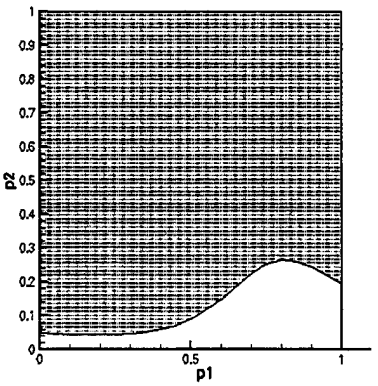

Level 5

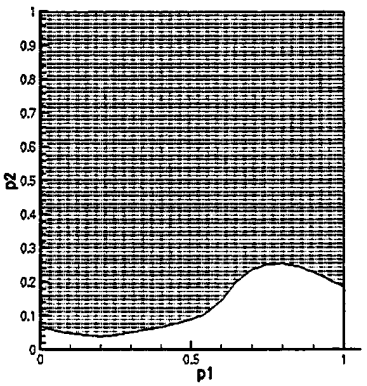

Level 6

The 0.2 threshold generates a failure region with very high-order geometry that standard FORM[6] and SORM[7] reliability-type methods (which can be applied to ascertain probability at this threshold level) cannot approximate very effectively. The Finite Element / Lattice Sampling (FE/LS) methodology requires at least 13 function evaluations (Level 4) before the approximation begins to resemble the actual failure region.

The results of direct and decoupled LHS Monte Carlo evaluation of probabilities are plotted in Figure 3.3 and listed in Table 1. The abscissa values 1 - 7 in the data represent the various levels of FE/LS response surface approximations, with the Level 7 representation being the exact function itself.

A very prominent "adjustment" in the convergence behavior depicted by Figure 3.3 occurs in going from Levels 3 to 4 at all population sizes. This adjustment corresponds to the markedly smaller shaded areas in Levels 2 and 3 vs. the other Levels. Level 1, though also having a grossly different configuration from the exact region, is fairly close in overall area, and the distribution of the area benefits coincidentally from the circular symmetry of the JPDF. A general (nonaxisymmetric) distribution combined with the Level 1 approximation would certainly not yield such close values to the exact. The large undulation in the Lattice Sampling convergence behavior is representative of the oscillatory convergence behavior normally exhibited by sampling methods. One thousand LHS samples appear to be enough for convergence of the exact result (Level 7), though results at some of the lower levels of approximation take an order of magnitude more samples to converge. This is a repeated result throughout much of this study: the lower the approximation Level, the more samples it usually takes for convergence.

For this test problem convergence of the progressive Lattice Sampling scheme appears to occur by Level 5 (25 samples) for all LHS populations.

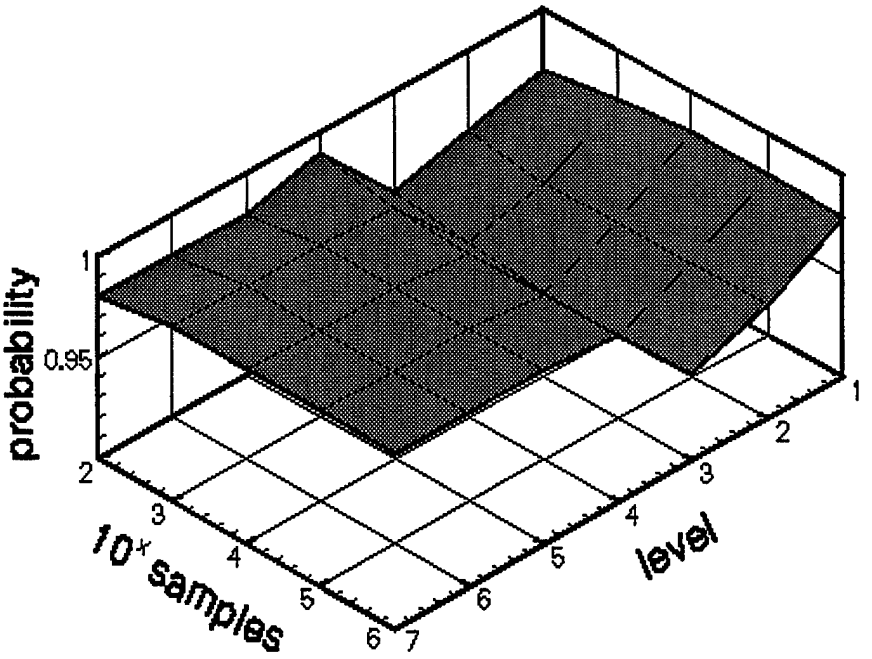

Figure 3.3 Convergence behavior for LHS Monte Carlo sampling and Progressive Lattice sampling for a threshold of 0.2.

Level of Approximation	Number of Latin Hypercube Monte Carlo Samples				
	10^2	10^3	10^4	10^5	10^6
1	0.97000	0.97600	0.98000	0.97936	0.97899
2	0.96000	0.95500	0.95580	0.95602	0.95608
3	0.95000	0.94600	0.94190	0.94093	0.94171
4	0.99000	0.98300	0.98110	0.98091	0.98112
5	0.98000	0.98600	0.98440	0.98461	0.98445
6	0.98000	0.98600	0.98380	0.98383	0.98388
7 (exact)	0.98000	0.98600	0.98460	0.98448	0.98439

Table 1 Probability of failure for various numbers of Latin Hypercube Monte Carlo samples of the exact function (Level 7) and successive FE/LS Levels (Func. 1, Threshold = 0.2). (These values are plotted above in Figure 3.3.)

3.3.2 Function 1, Threshold = 0.5

The shaded regions below signify the parameter space "failure regions" for various representations of Function 1 and a threshold exceedance value of 0.5.

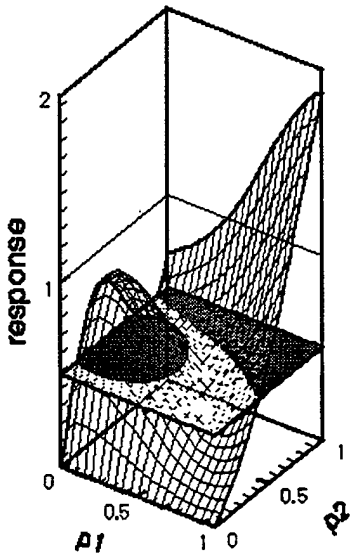

Exact Function cut by threshold plane of response = 0.5

Exact failure regions (shaded)

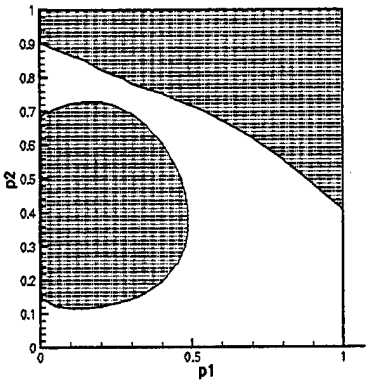

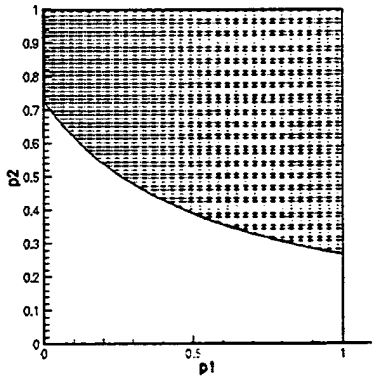

Level 1

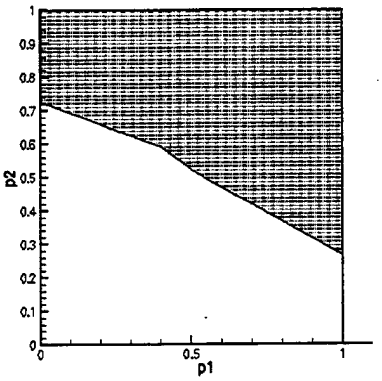

Level 2

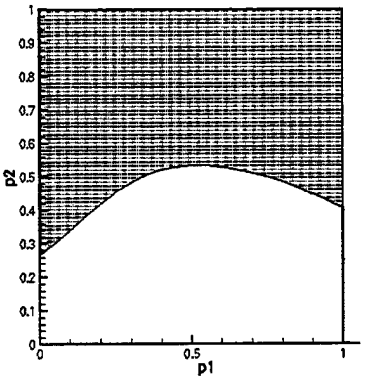

Level 3

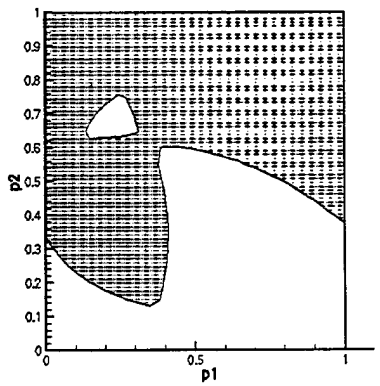

Level 4

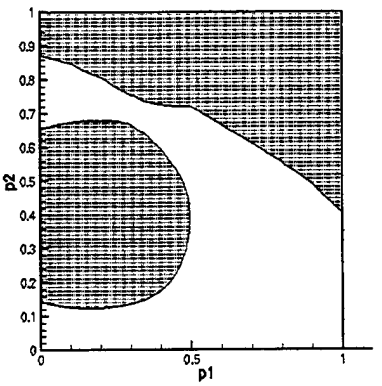

Level 5

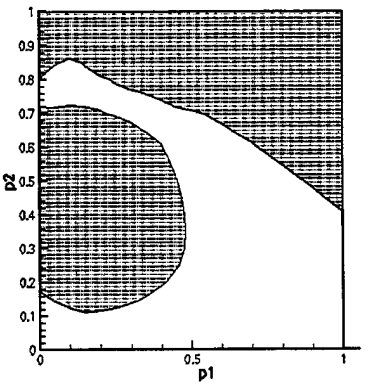

Level 6

This benchmark problem has two separate failure regions, one of which is a semicircular-like failure "island" of high-order geometry. Because of the disjoint regions and complexity of the geometry, reliability-type methods are not practical for assessing probability at the 0.5 threshold level. The FE/LS methodology requires about 25 FEVs (Level 5) before the approximate failure region begins to adequately resemble the exact one.

Figure 3.4 shows the convergence behavior for the 0.5 threshold. Table 2 lists the data. A trend of oscillatory convergence is observed, with the Level 6 results based on 41 FEVs being essentially converged to the probabilities from the exact function. The FE/LS method takes more samples to satisfactorily handle the complexity and multiplicity of the failure regions for this case versus the simple single region for the 0.2 threshold. For each of the global response surfaces (Levels 1 - 6) the LHS sampling converges in about 10,000 samples, demonstrating slight oscillatory convergence to that point. It may be remarked that the number of LHS samples required before convergence is established is generally an order or magnitude greater than for the 0.2 threshold. This is probably partially a result of the complexity and multiple-connectedness of the failure regions and of the fact that the total probability has decreased from an order of 1.0 for the 0.2 threshold to the order of 0.1 for this threshold.

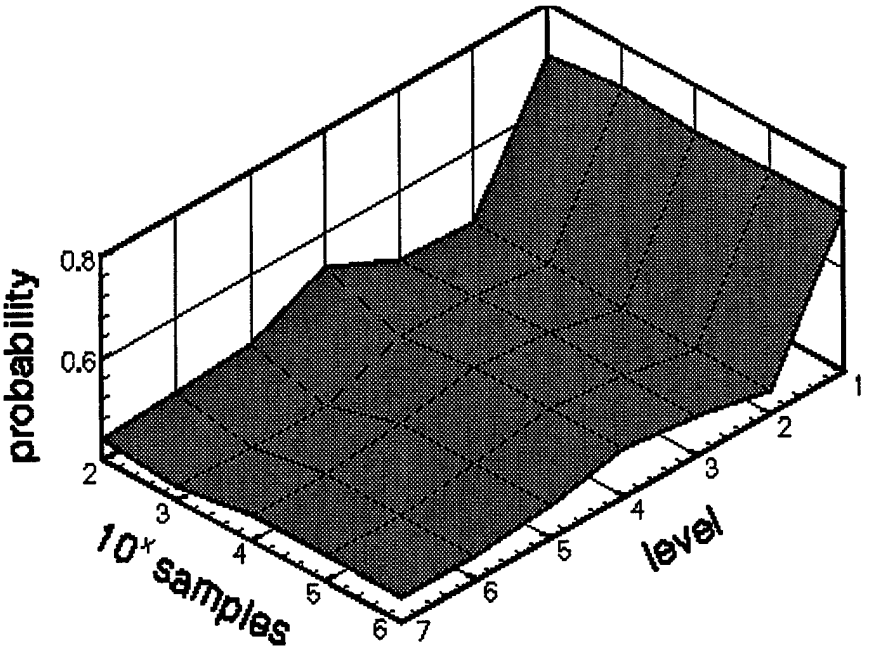

Figure 3.4 Convergence behavior for LHS Monte Carlo sampling and Progressive Lattice sampling for a threshold of 0.5.

		Number of Latin Hypercube Monte Carlo Samples				
		10^2	10^3	10^4	10^5	10^6
Level of Approximation	1	0.70000	0.71700	0.71070	0.71179	0.71374
	2	0.45000	0.45000	0.44290	0.44439	0.44574
	3	0.46000	0.47200	0.47910	0.47671	0.47708
	4	0.53000	0.47600	0.49570	0.49278	0.49371
	5	0.46000	0.42400	0.46790	0.46721	0.46592
	6	0.45000	0.42400	0.44850	0.44715	0.44587
	7 (exact)	0.44000	0.42900	0.45090	0.45058	0.44921

Table 2 Probability of failure for various numbers of Latin Hypercube Monte Carlo samples of exact function (Level 7) and successive FE/LS Levels (Function 1, Threshold = 0.5). (These values are plotted above in Figure 3.4.)

3.3.3 Function 1, Threshold = 1.0

The shaded regions below signify the parameter space "failure regions" for various representations of Function 1 and a threshold exceedance value of 1.0.

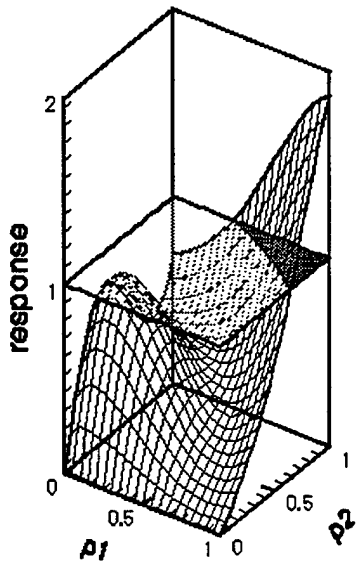

Exact Function cut by threshold plane of response = 1.0

Exact failure region (shaded)

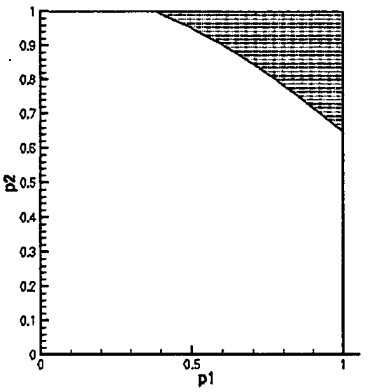

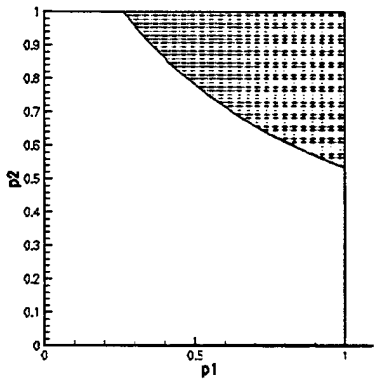

Level 1

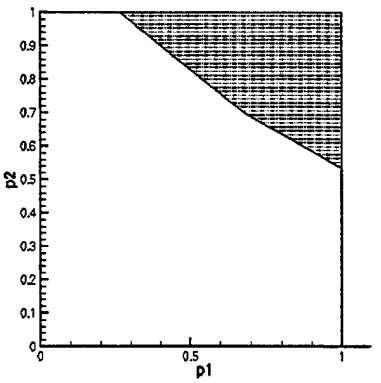

Level 2

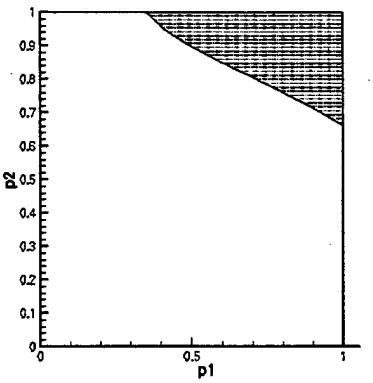

Level 3

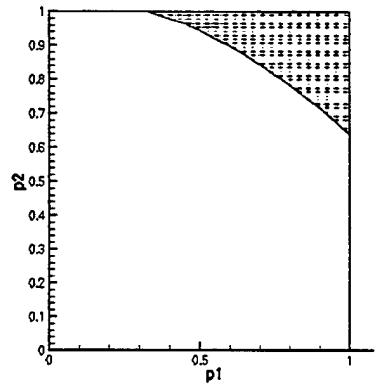

Level 4

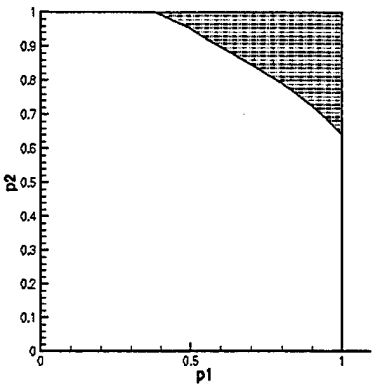

Level 5

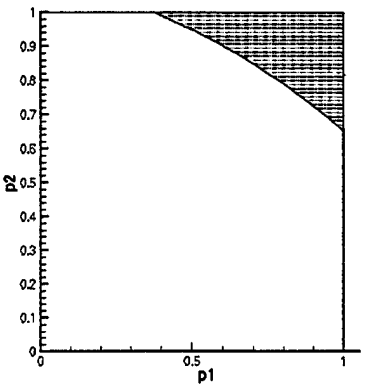

Level 6

The 1.0 threshold yields a failure region that is much more accommodating to reliability methods than the 0.2 and 0.5 thresholds do. The boundaries between 'failure' and 'no failure' would seemingly be adequately approximated as linear (FORM) or quadratic (SORM) curves. The FE/LS approximations at Level 4 (13 FEVs) and higher appear to do a good job of reproducing the exact failure region. This is verified in the convergence behavior plot Figure 3.5. Table 3 lists the corresponding data. Though the failure region is much simpler to resolve than for the 0.2 and 0.5 thresholds, 10,000 LHS samples are still required before veritable convergence occurs at all Levels of approximation. This is presumably because, though the failure region is easier to resolve in this case, the probability level drops to the order of 0.01. Again Monte Carlo convergence appears somewhat slower at the lower Levels of approximation than at the higher Levels.

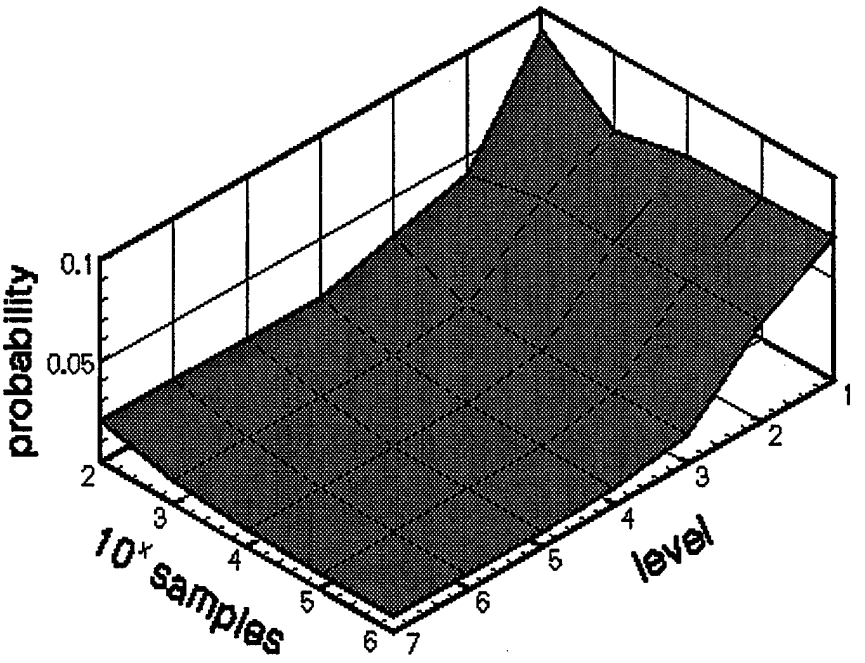

Figure 3.5 Convergence behavior for LHS Monte Carlo sampling and Progressive Lattice sampling for a threshold of 1.0.

Level of Approximation	Number of Latin Hypercube Monte Carlo Samples				
	10^2	10^3	10^4	10^5	10^6
1	9.0000e-02	6.1000e-02	6.9300e-02	6.9950e-02	7.0624e-02
2	4.0000e-02	4.9000e-02	4.7900e-02	4.9560e-02	4.9359e-02
3	3.0000e-02	1.6000e-02	1.4000e-03	1.4210e-02	1.3946e-02
4	2.0000e-02	1.2000e-02	9.3000e-03	8.2900e-03	8.1160e-03
5	2.0000e-02	1.2000e-02	8.2000e-03	7.5800e-03	7.3930e-03
6	2.0000e-02	1.2000e-02	8.1000e-03	7.3900e-03	7.2140e-03
7 (exact)	2.0000e-02	1.2000e-02	8.7000e-03	7.7600e-03	7.5600e-03

Table 3 Probability of failure for various numbers of Latin Hypercube Monte Carlo samples of exact function (Level 7) and successive FE/LS Levels (Function 1, Threshold = 1.0). (These values are plotted above in Figure 3.5.)

3.3.4 Function 1, Threshold = 1.5

The shaded regions below signify the parameter space "failure regions" for various representations of Function 1 and a threshold exceedance value of 1.5.

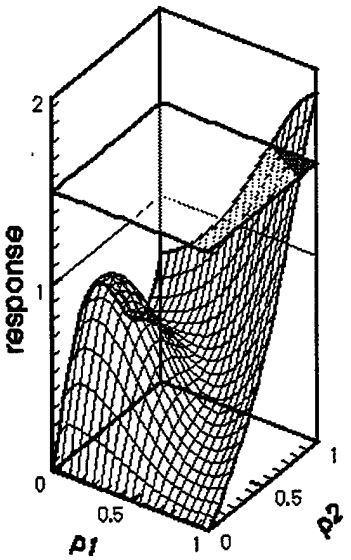

Exact Function cut by threshold plane of response = 1.5

Exact failure region (shaded)

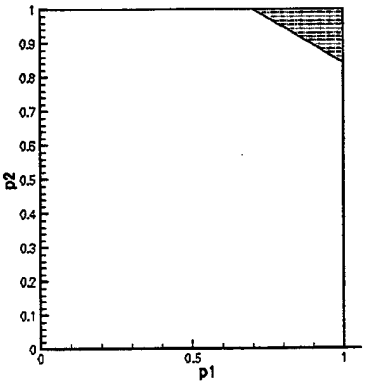

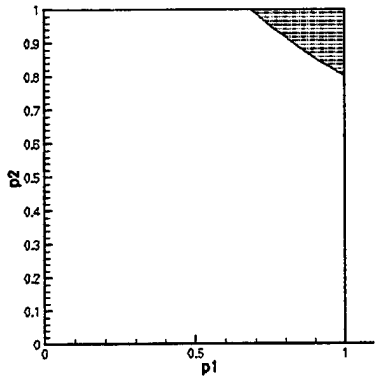

Level 1

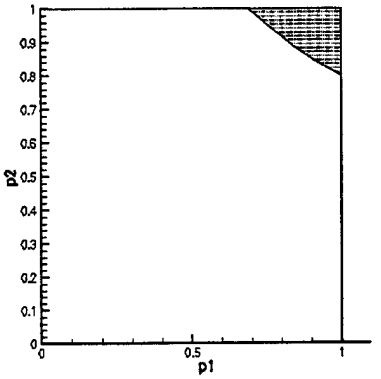

Level 2

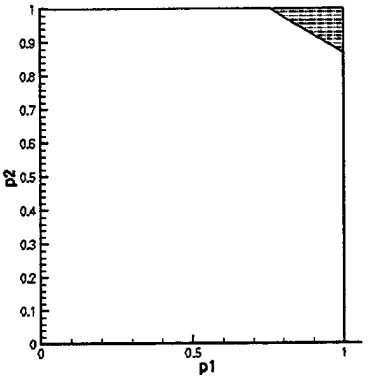

Level 3

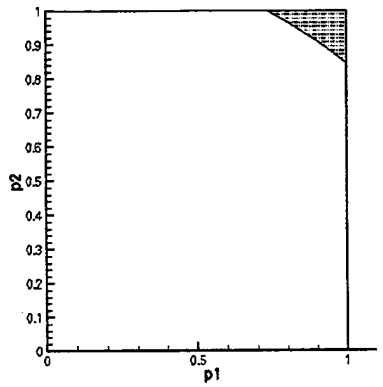

Level 4

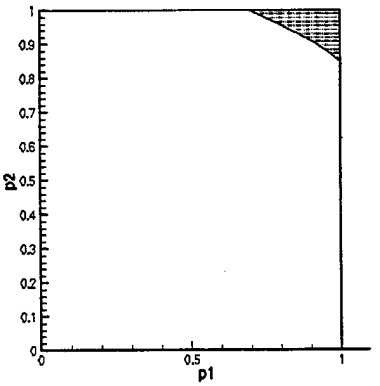

Level 5

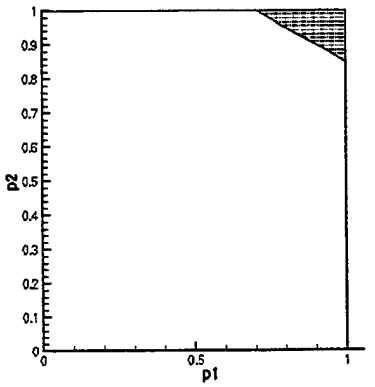

Level 6

The 1.5 threshold in Figure 3.6 also yields a failure region that reliability methods have an even chance of doing well on. Though the 1.5 threshold creates a failure region that would seem to be approximated adequately with 13 FEVs at Level 4, the convergence plot of Figure 3.6 reveals that, for the low probability of failure associated with this region, even the Level 6 representation with 41 FEVs does not appear to be quite adequate at some MC populations. Though the triangular failure region is seemingly very easy to resolve, even very small changes in the approximation can affect the number of LHS samples falling inside the region, and since the total number of samples falling in the region is relatively small (probability is on the order of 0.0001 for this problem), a small difference in the number of samples falling inside it can have a large relative effect. Again the effect is particularly accute at the lower levels of approximation where small inaccuracies in the size of the region (see Figure 3.6) contribute to relatively large percentage changes in its size and, therefore, in the number of samples falling within its boundaries. Also, the convergence of Monte Carlo sampling at a given Level of approximation is not as fast for this threshold as for the other thresholds. The results using the exact function (Level 7) do not seem to be converged even with 10^6 samples, though some of the other Levels look converged at this number of samples. The reason for the slow Monte Carlo convergence is, of course, the very low probabilities involved.

To be effectively resolved, problems like this one will require a transition from global FE/LS refinement to more local methods like might be found in adaptive finite element meshing. Algorithms for global and local refinement and their integration into efficient and versatile hybrid decoupled Monte Carlo algorithms are presently being devised and tested in associated LDRD research.

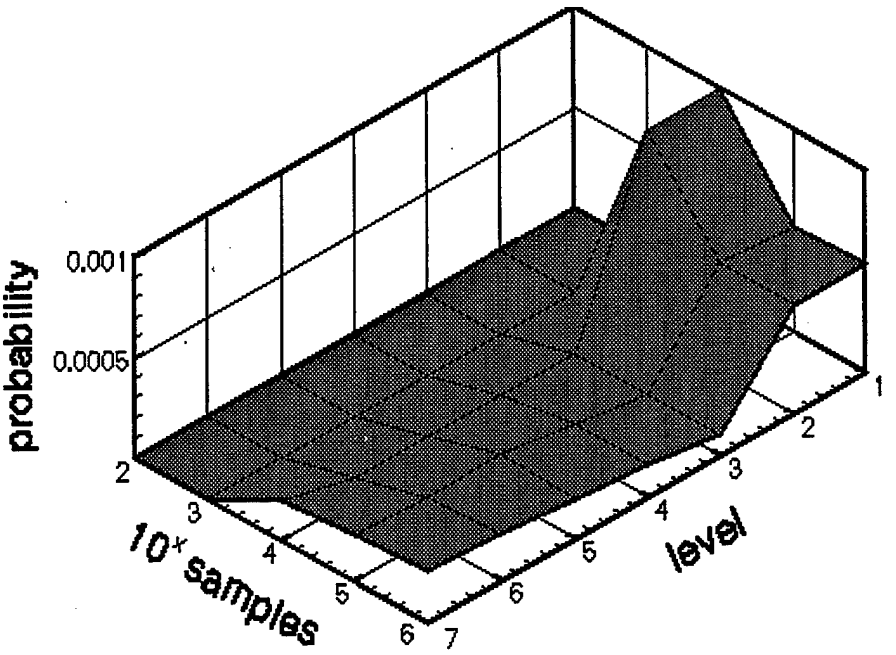

Figure 3.6 Convergence behavior for LHS Monte Carlo sampling and Progressive Lattice sampling for a threshold of 1.5.

Level of Approximation	Number of Latin Hypercube Monte Carlo Samples				
	10^2	10^3	10^4	10^5	10^6
1	0.0000	0.0000	1.0000e-03	5.1000e-04	5.3700e-04
2	0.0000	0.0000	1.0000e-03	5.5000e-04	5.4400e-04
3	0.0000	0.0000	1.0000e-04	1.0000e-04	1.0000e-04
4	0.0000	0.0000	1.0000e-04	1.6000e-04	1.5600e-04
5	0.0000	0.0000	1.0000e-04	2.2000e-04	1.9400e-04
6	0.0000	0.0000	1.0000e-04	2.1000e-04	2.2800e-04
7 (exact)	0.0000	0.0000	2.0000e-04	2.3000e-04	2.5200e-04

Table 4 Probability of failure for various numbers of Latin Hypercube Monte Carlo samples of exact function (Level 7) and successive FE/LS Levels (Function 1, Threshold = 1.5). (These values are plotted above in Figure 3.6.)

3.3.5 Function 2, Threshold = 0.05

The shaded regions below signify the parameter space "failure regions" for various representations of Function 2 and a threshold exceedance value of 0.05.

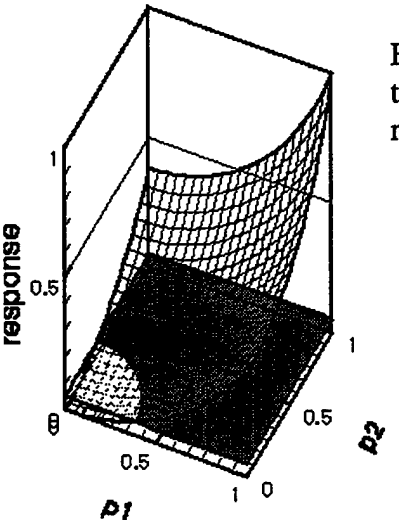

Exact Function cut by threshold plane of response = 0.05

Exact failure region (shaded)

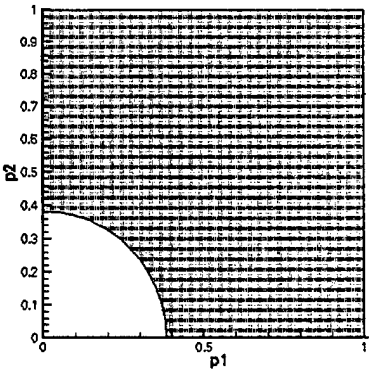

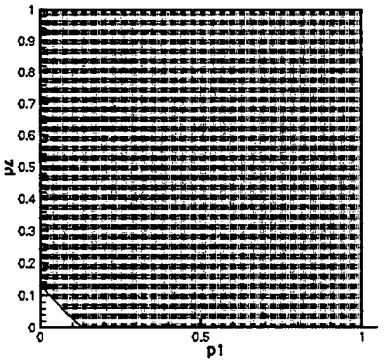

Level 1

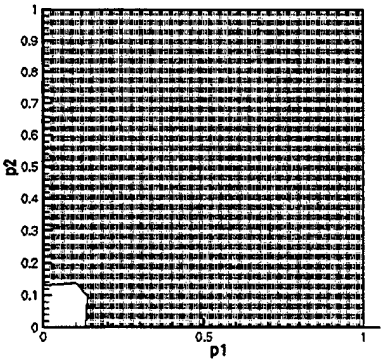

Level 2

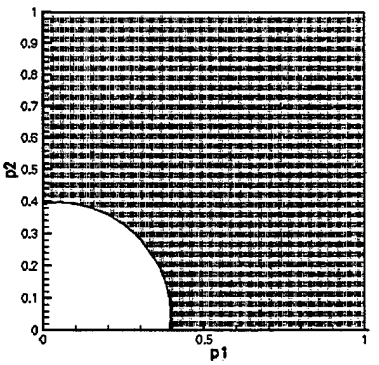

Level 3

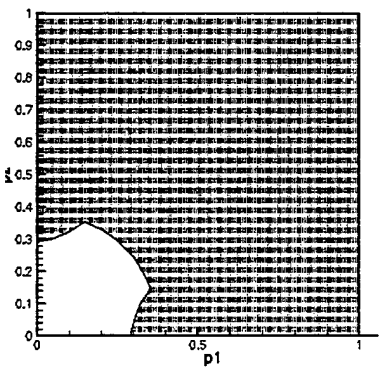

Level 4

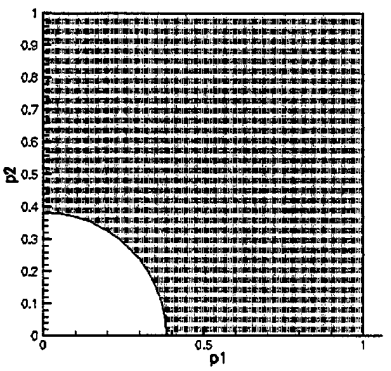

Level 5

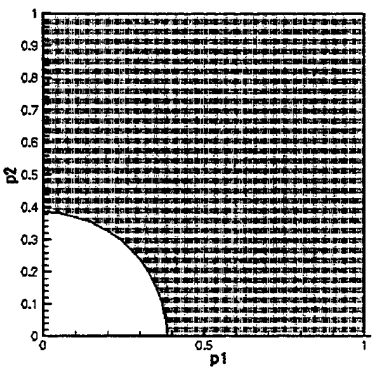

Level 6

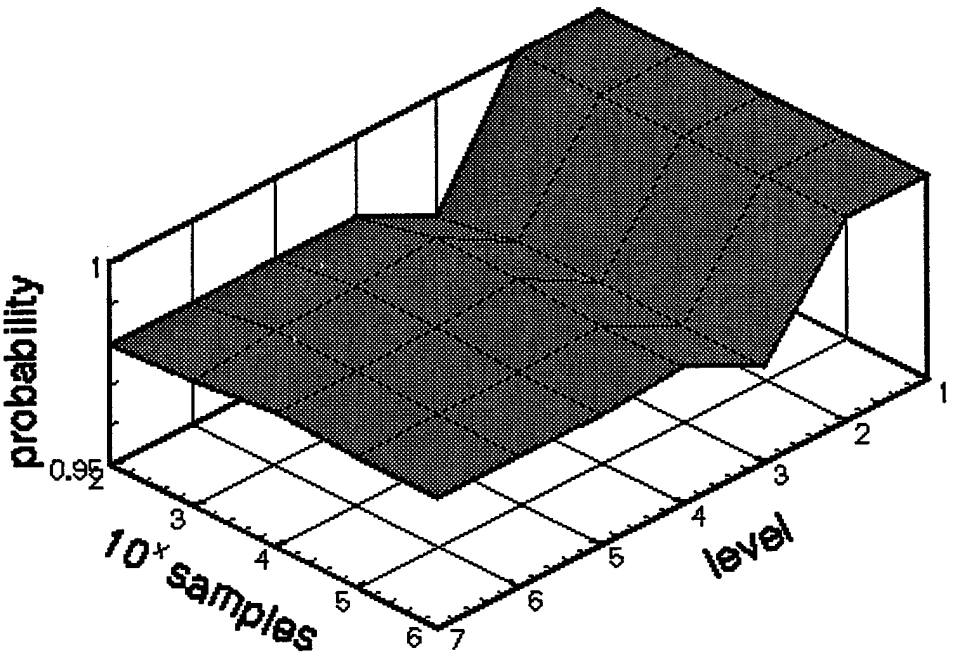

Figure 3.7 Convergence behavior for LHS Monte Carlo sampling and Progressive Lattice sampling for a threshold of 0.05.

Level of Approximation	Number of Latin Hypercube Monte Carlo Samples				
	10^2	10^3	10^4	10^5	10^6
1	1.0000	1.0000	1.0000	0.99998	0.99996
2	1.0000	1.0000	0.99960	0.99981	0.99979
3	0.97000	0.97410	0.97410	0.97368	0.97377
4	0.98000	0.98560	0.98560	0.98393	0.98374
5	0.98000	0.98360	0.98360	0.98267	0.98244
6	0.98000	0.98350	0.98350	0.98261	0.98235
7 (exact)	0.98000	0.98100	0.98360	0.98261	0.98235

Table 5 Probability of failure for various numbers of Latin Hypercube Monte Carlo samples of exact function (Level 7) and successive FE/LS Levels (Function 2, Threshold = 0.05). (These values are plotted above in Figure 3.7.)

3.3.6 Function 2, Threshold = 0.2

The shaded regions below signify the parameter space "failure regions" for various representations of Function 2 and a threshold exceedance value of 0.2.

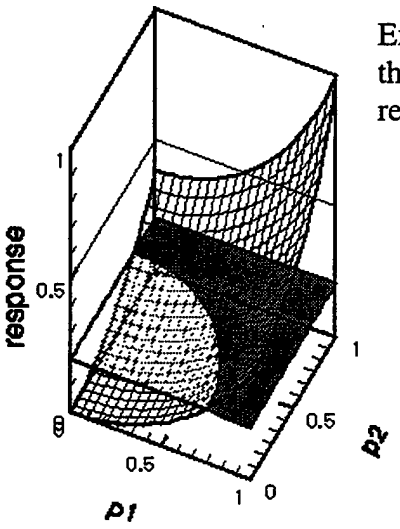

Exact Function cut by threshold plane of response = 0.2

Exact failure region (shaded)

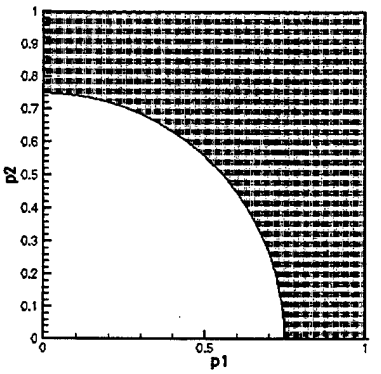

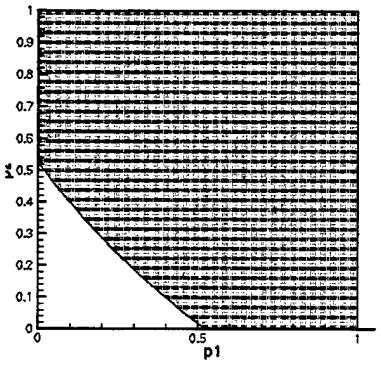

Level 1

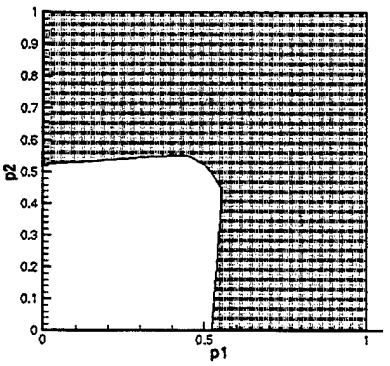

Level 2

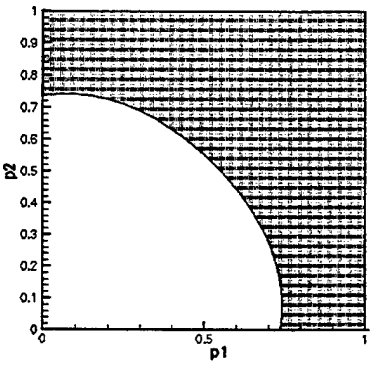

Level 3

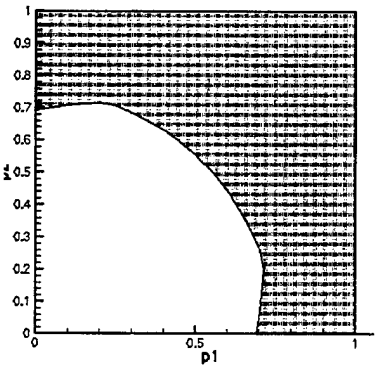

Level 4

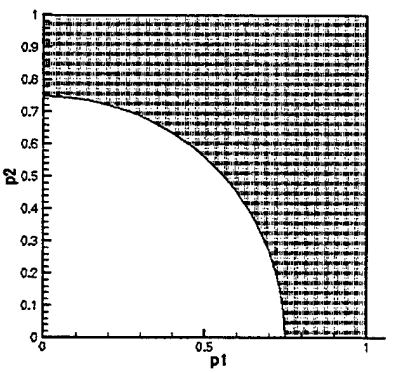

Level 5

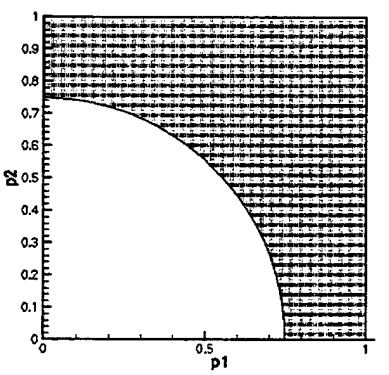

Level 6

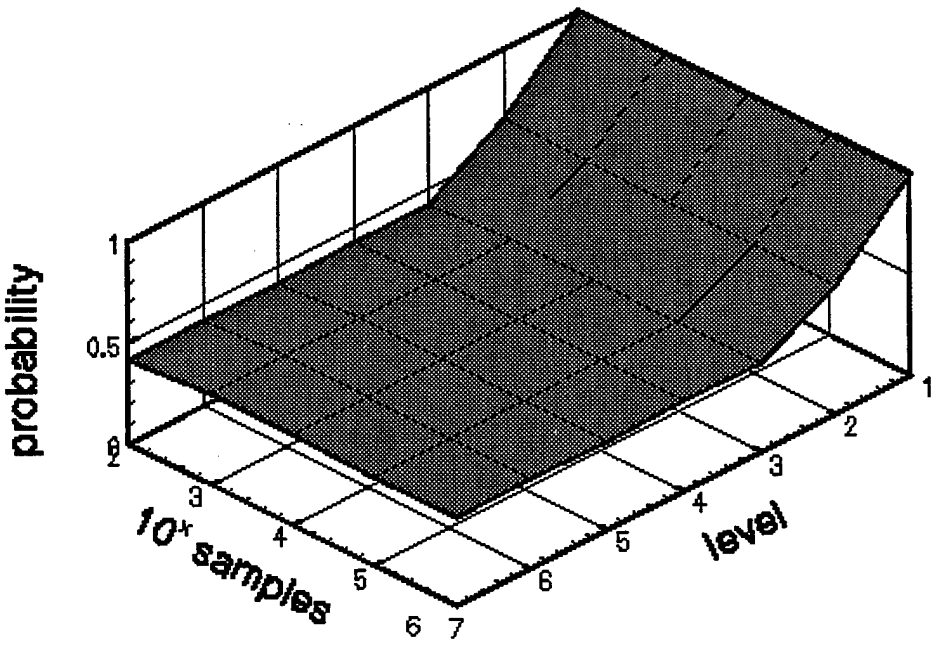

Figure 3.8 Convergence behavior for LHS Monte Carlo sampling and Progressive Lattice sampling for a threshold of 0.2.

Level of Approximation	Number of Latin Hypercube Monte Carlo Samples				
	10^2	10^3	10^4	10^5	10^6
1	0.99000	0.98500	0.98730	0.98607	0.98547
2	0.65000	0.64600	0.63580	0.64053	0.64095
3	0.42000	0.44880	0.44880	0.44685	0.44943
4	0.42000	0.45110	0.45110	0.44944	0.45194
5	0.41000	0.44160	0.44160	0.44005	0.44238
6	0.42000	0.44800	0.44800	0.44522	0.44780
7 (exact)	0.42000	0.44900	0.44720	0.44477	0.44737

Table 6 Probability of failure for various numbers of Latin Hypercube Monte Carlo samples of exact function (Level 7) and successive FE/LS Levels (Function 2, Threshold = 0.2). (These values are plotted above in Figure 3.8.)

3.3.7 Function 2, Threshold = 0.4

The shaded regions below signify the parameter space "failure regions" for various representations of Function 2 and a threshold exceedance value of 0.4.

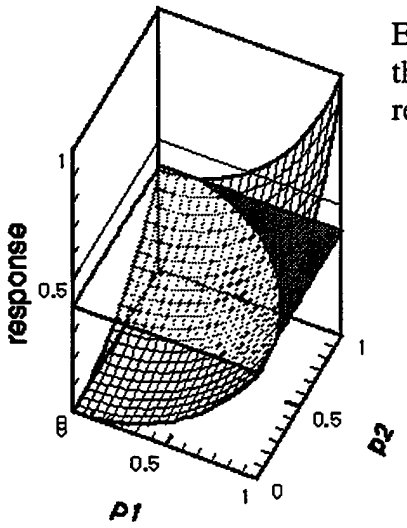

Exact Function cut by threshold plane of response = 0.4

Exact failure region (shaded)

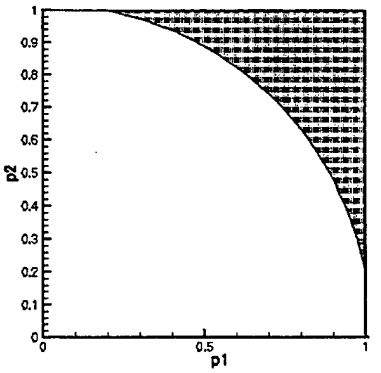

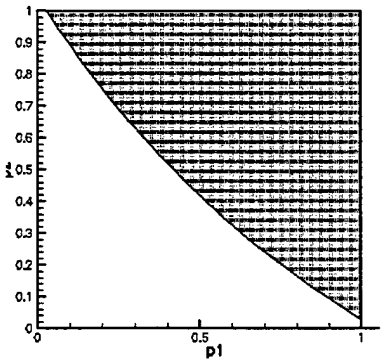

Level 1

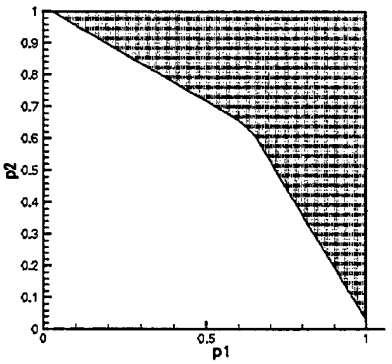

Level 2

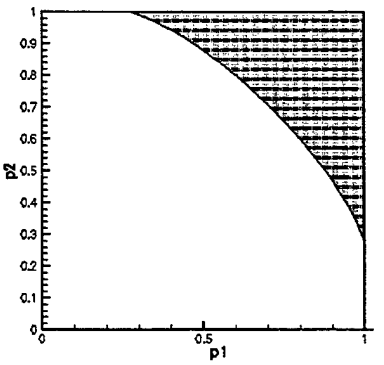

Level 3

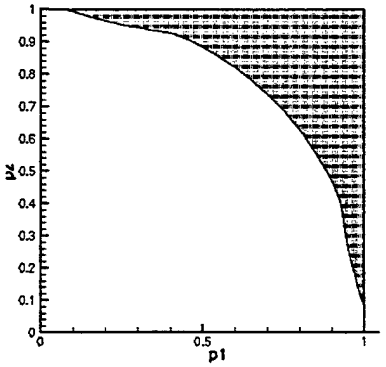

Level 4

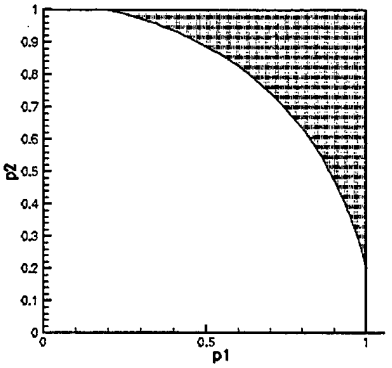

Level 5

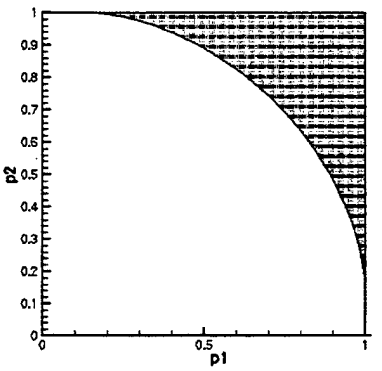

Level 6

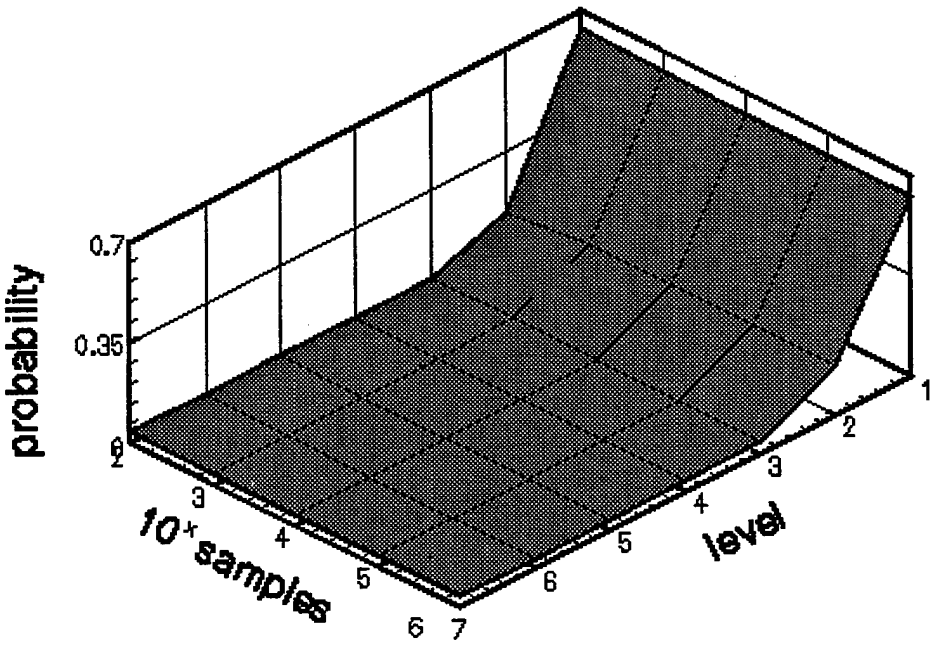

Figure 3.9 Convergence behavior for LHS Monte Carlo sampling and Progressive Lattice sampling for a threshold of 0.4.

Level of Approximation	Number of Latin Hypercube Monte Carlo Samples				
	10^2	10^3	10^4	10^5	10^6
1	0.64000	0.63000	0.62410	0.62586	0.62698
2	0.14000	0.16700	0.17040	0.17331	0.17228
3	4.0000e-02	4.5800e-02	4.5800e-02	4.5630e-02	4.5461e-02
4	4.0000e-02	3.9400e-02	3.9400e-02	3.9120e-02	3.8427e-02
5	4.0000e-02	3.6400e-02	3.6400e-02	3.5960e-02	3.5287e-02
6	4.0000e-02	3.5600e-02	3.5600e-02	3.5660e-02	3.5011e-02
7 (exact)	4.0000e-02	3.9000e-02	3.6600e-02	3.6350e-02	3.5670e-02

Table 7 Probability of failure for various numbers of Latin Hypercube Monte Carlo samples of exact function (Level 7) and successive FE/LS Levels (Function 2, Threshold = 0.4). (These values are plotted above in Figure 3.9.)

3.3.8 Function 2, Threshold = 0.6

The shaded regions below signify the parameter space "failure regions" for various representations of Function 2 and a threshold exceedance value of 0.6.

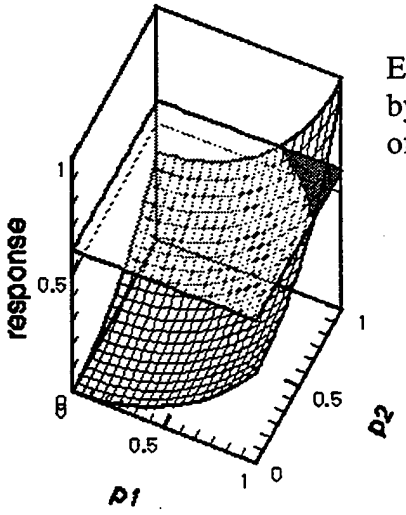

Exact Function cut by threshold plane of response = 0.6

Exact failure region (shaded)

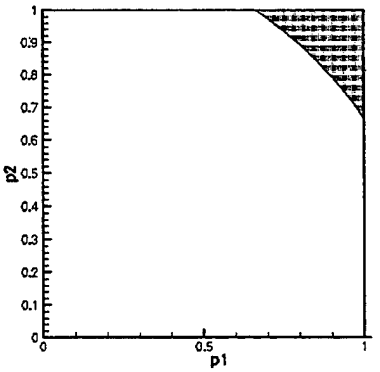

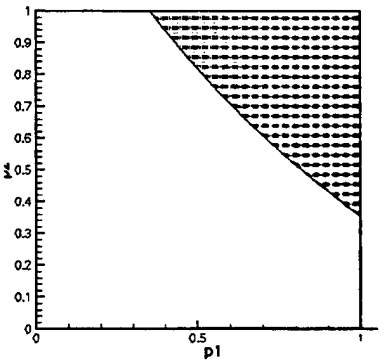

Level 1

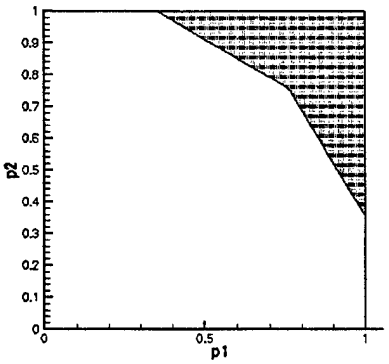

Level 2

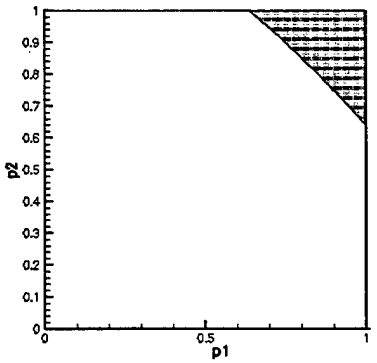

Level 3

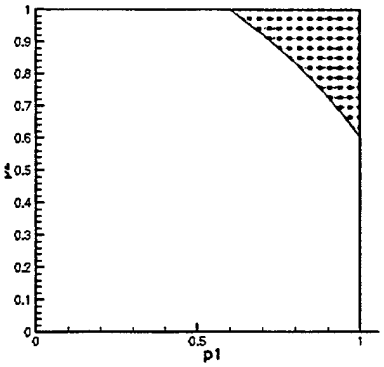

Level 4

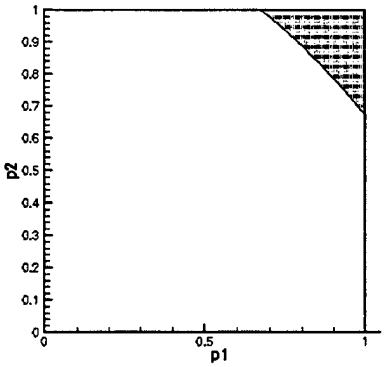

Level 5

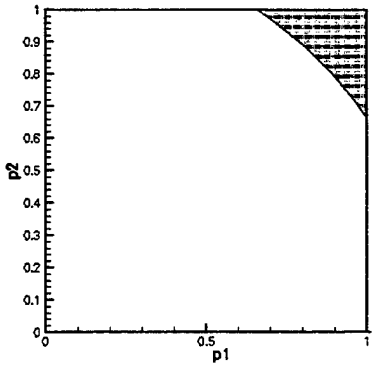

Level 6

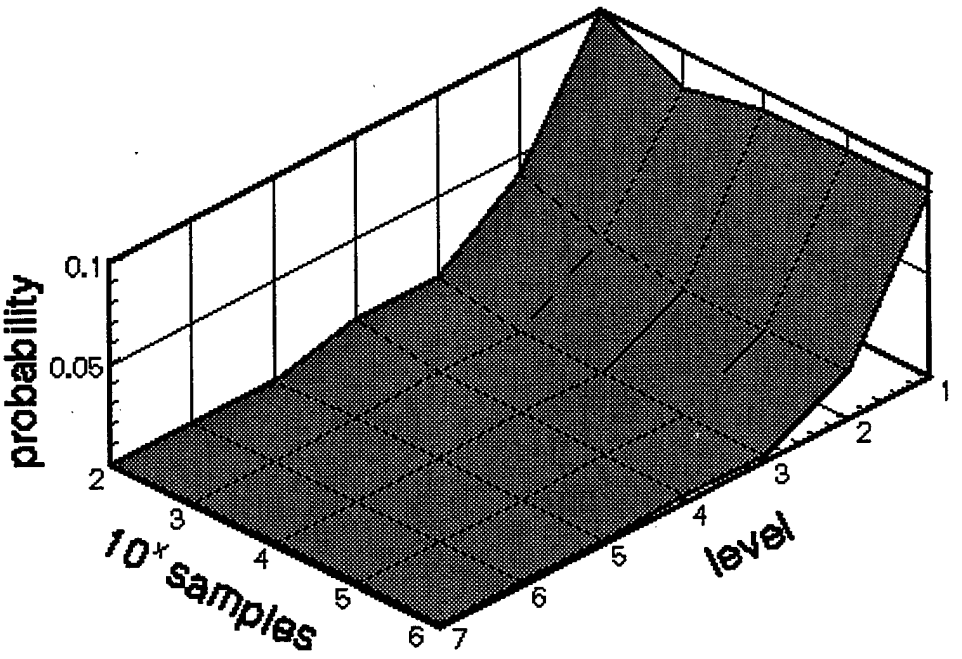

Figure 3.10 Convergence behavior for LHS Monte Carlo sampling and Progressive Lattice sampling for a threshold of 0.6.

Level of Approximation	Number of Latin Hypercube Monte Carlo Samples				
	10^2	10^3	10^4	10^5	10^6
1	1.0000e-01	8.2000e-02	9.0300e-02	9.1060e-02	9.1197e-02
2	4.0000e-02	2.9000e-02	2.3300e-02	2.3660e-02	2.3120e-02
3	1.0000e-02	2.6000e-03	2.6000e-03	2.1800e-03	2.1990e-03
4	1.0000e-02	4.0000e-03	4.0000e-03	3.2000e-03	3.1050e-03
5	0.0000	1.8000e-03	1.8000e-03	1.3200e-03	1.2800e-03
6	0.0000	1.7000e-03	1.7000e-03	1.2800e-03	1.2360e-03
7 (exact)	0.0000	1.0000e-03	1.7000e-03	1.2100e-03	1.1850e-03

Table 8 Probability of failure for various numbers of Latin Hypercube Monte Carlo samples of exact function (Level 7) and successive FE/LS Levels (Function 2, Threshold = 0.6). (These values are plotted above in Figure 3.10.)

As the figures presented in Sections 3.3.4 - 3.3.8 verify, the failure boundaries for all threshold levels are circular arcs (recall that Function 2 is a portion of a sphere). Level 3 (nine FEVs of the FE/LS methodology) appears to capture these arcs well. The Level 4 approximations (13 FEVs) appear in all cases to actually be worse than the Level 3 approximations, with the Level 5 (25 FEVs) and Level 6 (41 FEVs) approximations appearing nearly exact to the eye.

In terms of probabilities calculated at each of the threshold levels, the convergence plots Figure 3.7 - Figure 3.10 show that Monte Carlo results generally stabilize by Level 3 (nine FEVs). The most notable exception occurs for the 0.05 threshold in Figure 3.7. Counterintuitively, though the Level 4 (13 FEVs) approximation shown in Section 3.3.5 appears much worse than the Level 3 (nine FEVs) approximation for this threshold, the Level 4 approximation yields a much more accurate probability result from Monte Carlo sampling. This can be explained from the circular-normal nature of the JPDF being sampled and the better resolution in the Level 4 approximation of the portion of the non-failure region nearest the center of the distribution, which is most important to resolve since this region is sampled more than the extremeties of the non-failure region. Thus, *in these matters it is important to consider both the accuracy of the approximate response surface and the spatial importance of the accuracy as weighted by the spatial density in the JPDF.* Another notable exception occurs for a threshold of 0.6 at the lowest number of samples (100) where substantial corrections occur through Level 5. Though corrections are perceptible through Level 5 at the higher population sizes, the corrections are not as significant as at lower population sizes, in keeping with the trend already noted for Function 1.

Generally the results for Function 2 are essentially converged for all Levels at even the lowest population size of 100 samples. At populations of 10^4 to 10^6 samples no perceptible differences in results exist.

3.4 Efficiency Comparison of Decoupled and Direct MC Sampling

Toward a valid comparison of the convergence rates of direct and decoupled LHS Monte Carlo approaches, the following reasoning was used to establish a basis for comparison. Over the convergence plots Figures 3.3 - 3.10, a population size of 10,000 samples in all cases gives essentially the "exact" probabilities obtained with 1,000,000 samples. Therefore, 10^4 is taken as the convergence limit of population size for these problems. Assuming that each sample takes 1 second of CPU time (which is actually about 2 orders of magnitude longer than we experienced running the FE/LS INTERP code on these 2-random-variable problems), we arrive at a total execution time of 2.78 hours. Let us also assume that we have a large finite element model that takes an average of 2.78 CPU hours for each function evaluation in our problem. Therefore, to achieve a Level 1 decoupled Monte Carlo (10,000 sample) estimation of failure probability, we add the time required for the 4 FEVs in Level 1 to an equivalent 1 FEV of CPU time required to sample the Level 1 response surface 10,000 times via the INTERP code. Thus, the total equivalent CPU time for the analysis is 4 + 1 = 5 FEVs. We can then compare the results of 5 FEVs used in this manner to the results of using 5 FEVs in a direct Monte Carlo evaluation of probability. Analogously, a Level 6 analysis requires 41 + 1 = 42 FEVs, which we can compare against direct Monte Carlo evaluation with 42 samples.

Now, if the finite element model only takes an average of one CPU minute to run, then 167 of these can be run in the time it takes to run 10,000 one-CPU-second samples of the INTERP code. Thus, a Level 1 decoupled FE/LS Monte Carlo analysis requires 4 FEVs + the equivalent of 167 FEVs to sample INTERP 10,000 times, for a total equivalent of 4 + 167 = 171 FEVs. Thus, we should seek to compare the results of 171 direct Monte Carlo FEVs against 4 FEVs to set up Level 1 + 10,000 MC samples of the Level 1 response surface. By analogy, a Level 6 analysis implies the equivalent of 41 + 167 = 208 direct MC samples.

We see that for decoupled Monte Carlo analysis at a given FE/LS approximation Level, the equivalent number of direct MC samples decreases as the CPU time of the involved model increases -*e.g.*, from 171 to 5 and from 208 to 42- when model FEVs increase from 1 CPU minute to 2.78 CPU hr per evaluation. Therefore, *everything else being equal, relative to direct Monte Carlo analysis the marginal efficiency of the Finite Element / Lattice Sampling decoupled Monte Carlo (FELSDMC) approach increases as the size of the finite element model increases, which is a very favorable indicator for the FELSDMC method.*

The *absolute* efficiencies of the direct and decoupled LHS Monte Carlo approaches can be compared for the parameters of the present problems by examining Figures 3.11 - 3.14 (corresponding to the different thresholds applied to Function 1) and Figures 3.15 - 3.18 (corresponding to the different thresholds applied to Function 2). The abscissa in the plots are mapped in Table 9 to equivalent numbers of FEVs. The circles on the plots mark data generated by the FELSDMC method. The triangles on the plots mark data generated by direct Monte Carlo sampling where it is assumed that the model takes 60 times as long to run as the response surface approximation does. On the plots X marks the data generated by direct Monte Carlo sampling with a model assumed to take even 60 times longer still. In all cases (for all functions and threshold or probability levels), the FELSDMC method converges fastest toward the "exact" result obtained from 10,000 samples of the analytic function. The next fastest convergence rate occurs for direct MC sampling where FEVs are assumed to take one CPU minute (relative to

		Equivalent Number of FEVs			
		DMCFELS w/10^4 1-sec. MC samples	direct LHS (2.78 hr. CPU model)	DMCFELS w/10^4 1-sec. MC samples	direct LHS (1min. CPU model)
stage	1	5	5	5	171
	2	6	6	6	172
	3	10	10	10	176
	4	14	14	14	180
	5	26	26	26	192
	6	42	42	42	208

Table 9 Mapping of abscissa in Figures 3.11 - 3.18 to equivalent numbers of function evaluations.

one CPU second assumed per run of the INTERP code). Despite the slower convergence the equivalent computational costs shown in Table 9 are from 5 to 43 times the cost of the decoupled Monte Carlo approach. The slowest convergence occurs under the assumption that FEVs take 2.78 CPU hours each, in which case the direct Monte Carlo equivalent costs shown in the table are from 2% to 25% more than decoupled MC even though convergence is much slower. The data also suggests that the convergence advantages of the FELSDMC method become more pronounced as the magnitude of the probability being resolved decreases. This is to be expected for the smooth, non-stochastic, low-order functions tested here.

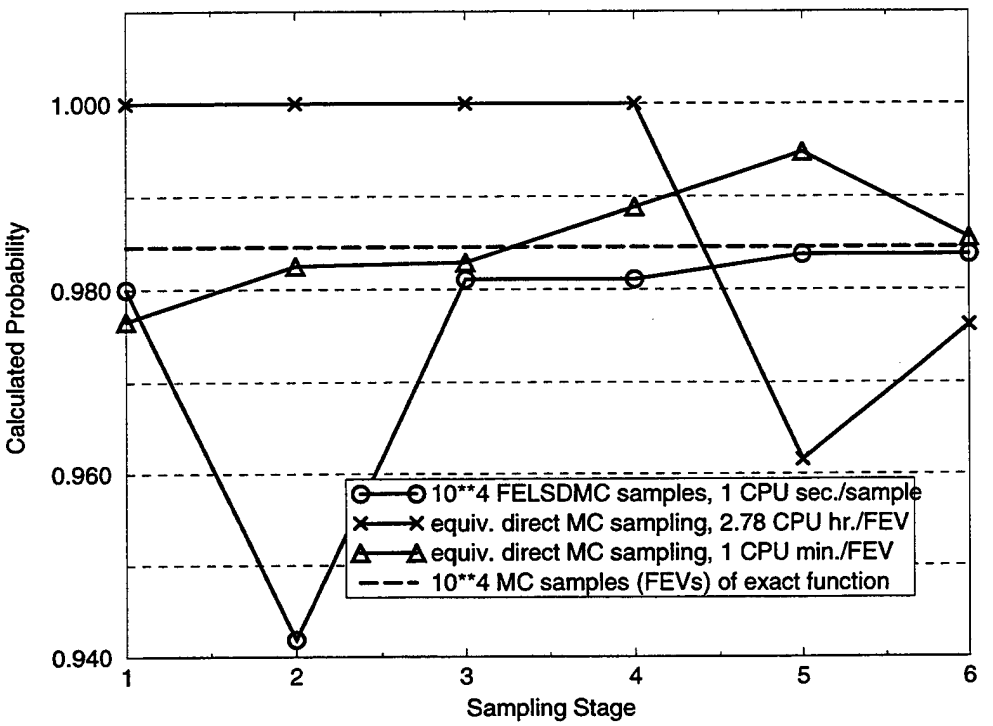

Figure 3.11 Comparison of various instances of direct and decoupled Monte Carlo Latin Hypercube Sampling for a threshold of 0.2, Function 1.

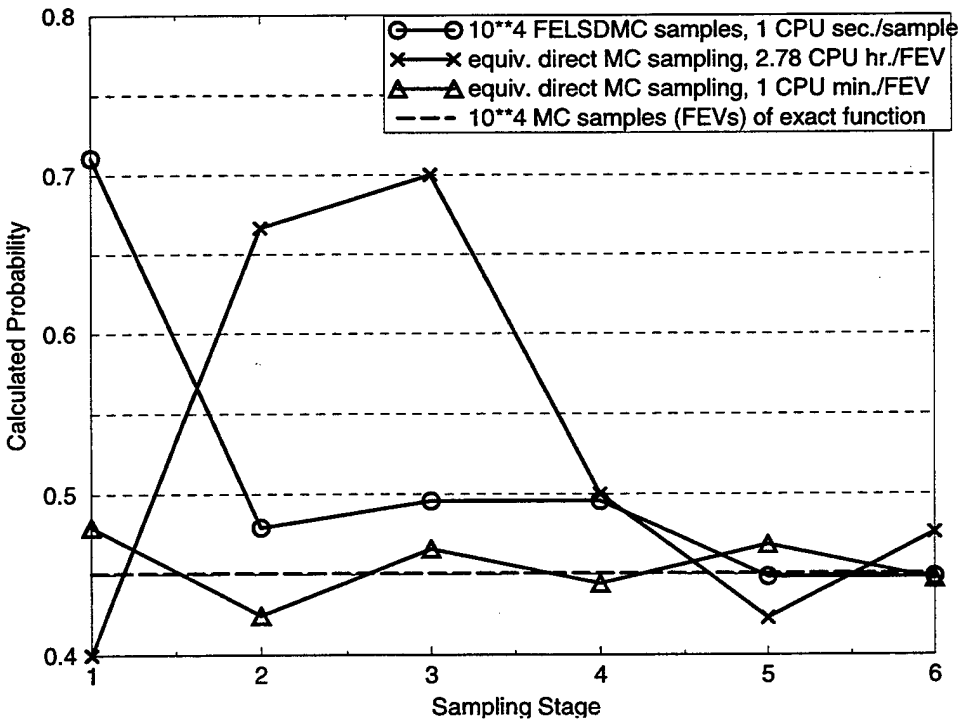

Figure 3.12 Comparison of various instances of direct and decoupled Monte Carlo Latin Hypercube Sampling for a threshold of 0.5, Function 1.

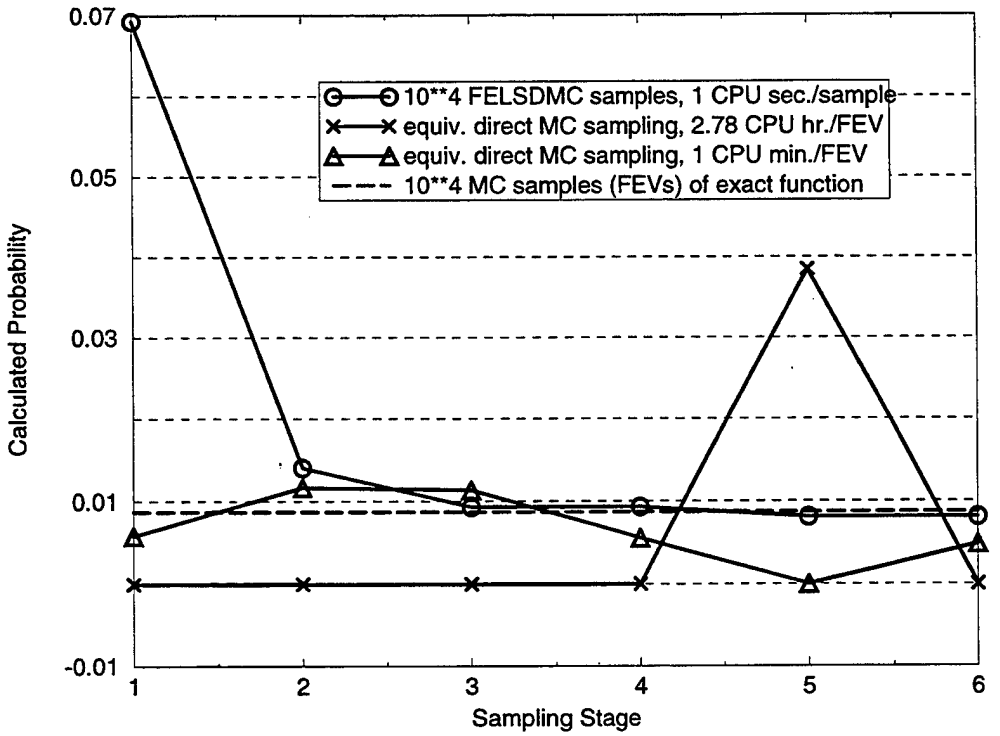

Figure 3.13 Comparison of various instances of direct and decoupled Monte Carlo Latin Hypercube Sampling for a threshold of 1.0, Function 1.

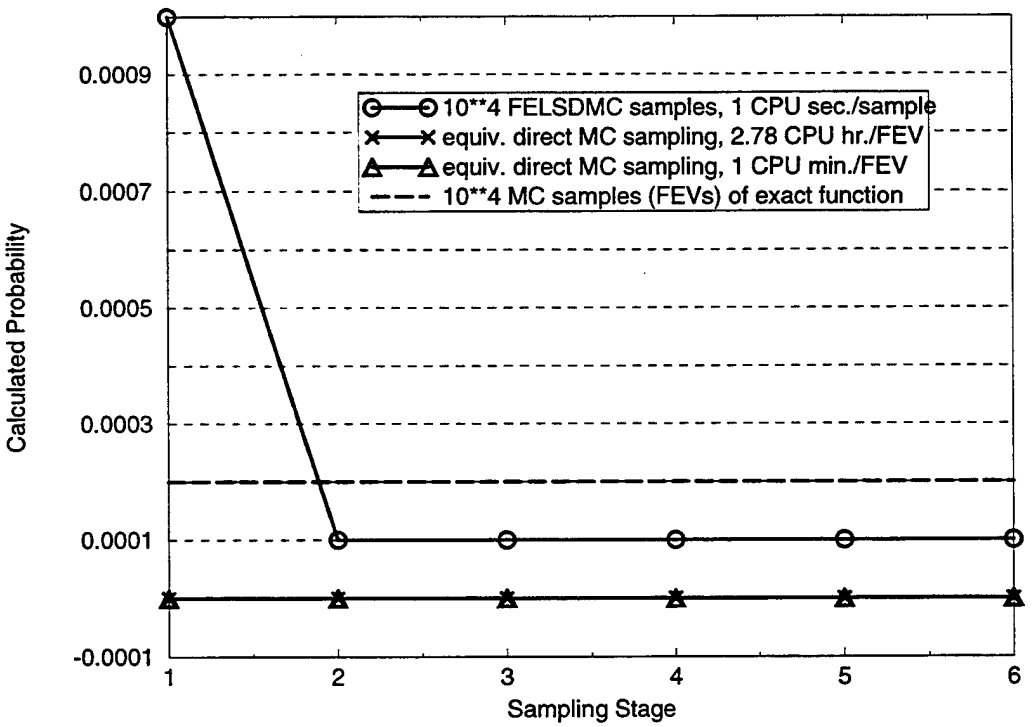

Figure 3.14 Comparison of various instances of direct and decoupled Monte Carlo Latin Hypercube Sampling for a threshold of 1.5, Function 1.

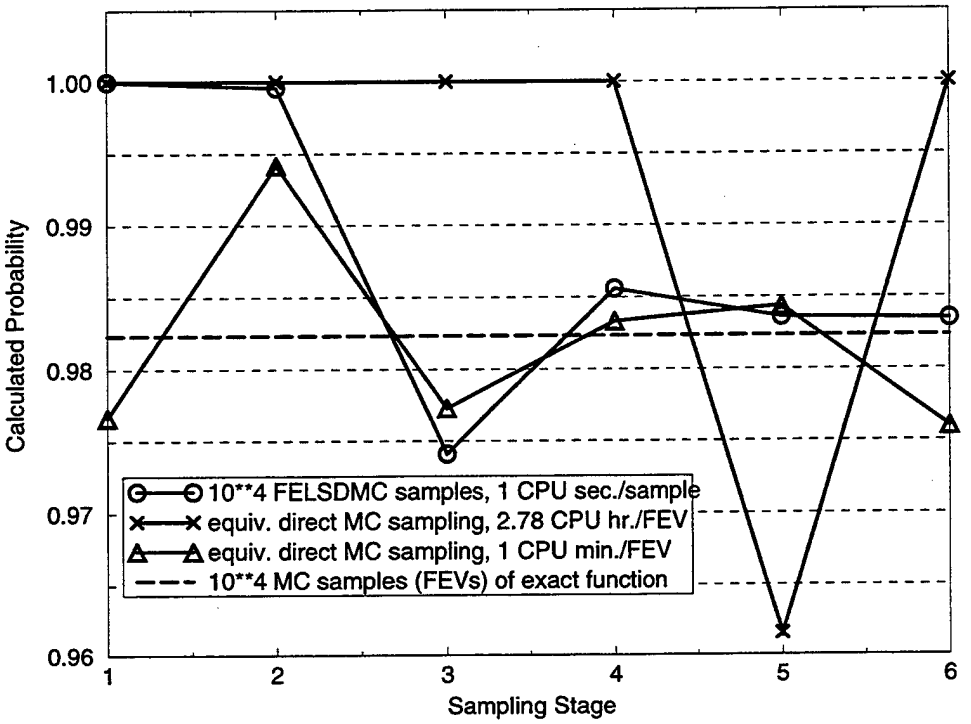

Figure 3.15 Comparison of various instances of direct and decoupled Monte Carlo Latin Hypercube Sampling for a threshold of 0.05, Function 2.

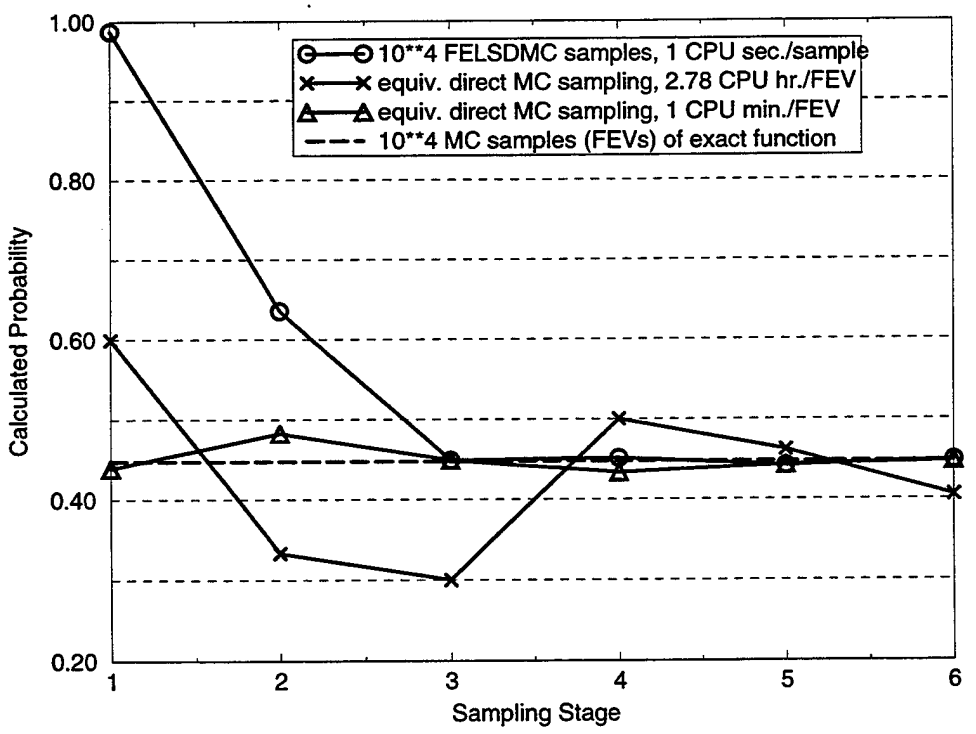

Figure 3.16 Comparison of various instances of direct and decoupled Monte Carlo Latin Hypercube Sampling for a threshold of 0.2, Function 2.

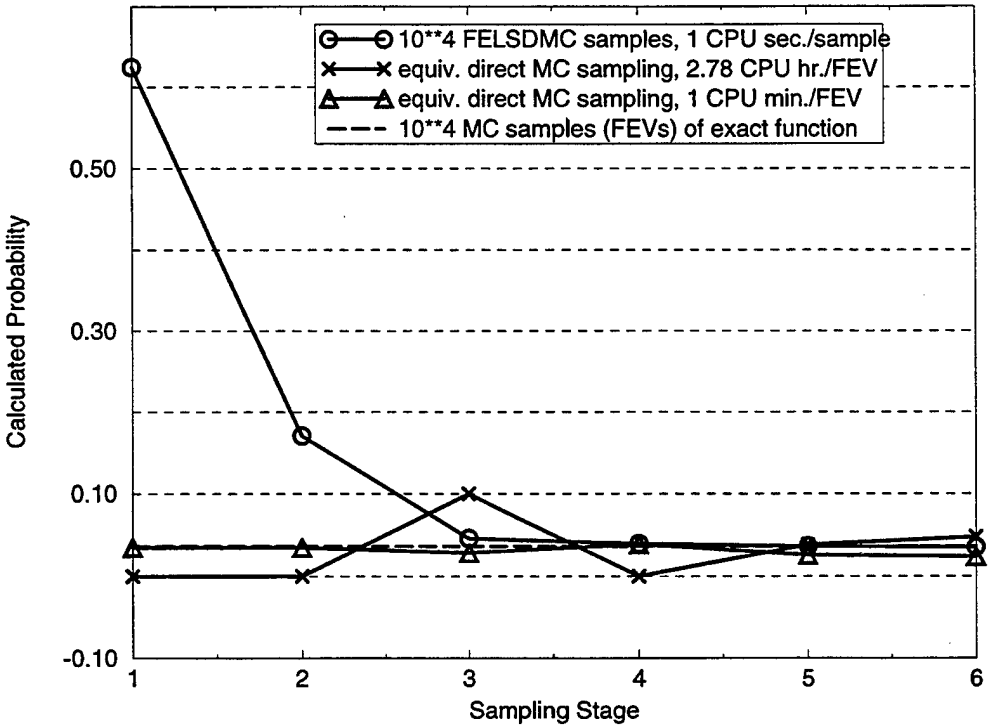

Figure 3.17 Comparison of various instances of direct and decoupled Monte Carlo Latin Hypercube Sampling for a threshold of 0.4, Function 2.

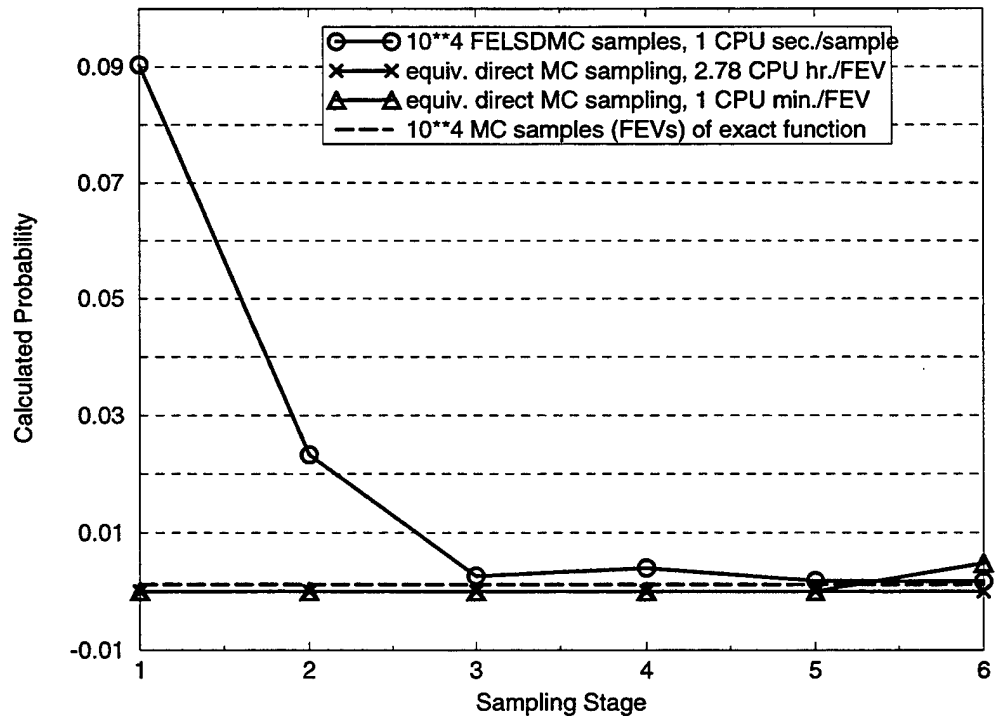

Figure 3.18 Comparison of various instances of direct and decoupled Monte Carlo Latin Hypercube Sampling for a threshold of 0.6, Function 2.

3.5 Conclusions

The results in this report indicate that geometry convergence in the Finite Element / Lattice Sampling scheme (*i.e.*, convergence of the FE/LS response surface to the topology of Functions 1 and 2) occurs with up to 5 orders of magnitude (but more typically from 1 to 3 orders of magnitude) less samples than it takes for LHS Monte Carlo sampling to converge to a stable probability estimate. In all cases the Level 6 approximations based on 41 samples approximated the exact analytic surfaces and corresponding mapped failure regions very well. In many cases only nine samples in the form of the Level 3 approximation were needed. In the usual case where it takes orders of magnitude more CPU time to run a simulation with the phenomenological model than to run the FE/LS response-surface code INTERP, the decoupled Monte Carlo FE/LS approach can require orders of magnitude less computer time overall than direct Monte Carlo analysis, with no appreciable loss of accuracy. Therefore, according to the many and varied tests applied here, it is more efficient to expend computer-model function evaluations on the building of the FE/LS response surface than to expend them in a direct Monte Carlo evaluation. Furthermore, the efficiency of the FELSDMC approach relative to the direct MC approach increases as the size of the computer model increases, and the convergence advantages of the FELSDMC method seem to become more pronounced as the magnitude of the probability being resolved decreases. Both of these trends are very favorable indicators for the FELSDMC method.

4 Summary, Discussion, and Open Research Issues

The concept of building piecewise-continuous finite element response surfaces based on structured sampling was introduced. Preliminary investigation suggests that finite element implementations similar to the ones described here can be extended to N-dimensional problems and applied to other types of sampling paradigms yet to be explored in a FE response-surface context (such as classical experimental design). Additionally, the finite element representation of response surfaces allows for the construction of "random fields" that represent the uncertainty in the response surface itself due to multiple responses at a given set of parameters. This may occur, for example, when the same experiment is run several times under the same set of controlled parameters, with slightly different results each time due to uncontrollable factors or instrumentation and measurement uncertainties. Analogously, many different model responses can result for one set of controlled parameters if Monte Carlo analysis is used to sample the effects of modeling and numerical uncertainties in the underlying model.

Finite Element response surfaces based on Lattice Sampling (one particular type of structured sampling) were found to be very effective in association with decoupled Monte Carlo analysis for probability estimation. Two very different test functions were tried, representing a large range of probabilities (from 10^{-4} to order 1) and very demanding failure region geometries, so a large portion of the parameter space was investigated in this regard. However, the robustness of the FELSDMC method in the presence of non-normal random variables was not investigated.

Since a property of Lattice Sampling is uniform global coverage of the parameter space, it is not expected that a degradation in performance will occur for non-normal joint probability density functions. On the contrary, it may be that Lattice Sampling places samples too uniformly over the domain. Since in most cases, and particularly with normal JPDFs, Monte Carlo samples of the FE/LS response surface will occur more frequently in the middle of the parameter space and less at the edges, it makes sense that the sampling method should in most cases resolve the response surface better near the center and less well near the edges. Other structured sampling methods based in numerical quadrature, such as Patterson[7], Gauss, and Lobatto point location [8], tend to cover the center of the parameter space better than the edges. Thus, these could ultimately be superior to Lattice Sampling for global response surfaces. However, of all of these only Lattice Sampling has a fractal property[1] that allows straightforward and easy sub-grid refinement for local adaptivity in later rounds of local optimization and nondeterministic analysis.

A related research issue of fundamental importance is that of when to switch from the global phase of such problems to the local phase where local adaptive sampling is used to

[1] At any stage in the subdivision of the parameter space into finite elements, a given region encompassed within a finite element or group of finite elements can by isolated for further sampling and resolution by repeated halving of triangular finite elements and treating square elements or subelements like Level 1 or 4, whichever applies, and then proceeding to subdivide by progressing through the Levels displayed in Figure 2.1 until sufficient refinement of the area of interest has occurred (to do this, INTERP1C can be called recursively).

accelerate convergence to local optima or to a probability result. Given a target or budget number of samples (FEVs with a computer model or experiments to run), how should they be divided between the global and local phases of the problem such that the optimal (most accurate or global) result is obtained? Establishment of "rules of thumb" for optimal ratios of global to local FEVs will take much investigation and is expected to be very problem dependent. Additionally, the best options for local adaptive sampling are at this point unclear. The fractal character of Lattice Sampling is useful for multigrid adaptivity by subgrid refinement, but this type of adaptivity can be somewhat inefficient because of the requirement to incrementally add a matrix of sample points, rather than just one new sample point at a time. These issues will be explored in the future under the same LDRD that funded this work.

Of what was established in this work, the geometry convergence in the Finite Element / Lattice Sampling scheme (*i.e.* convergence of the FE/LS response surface to the topology of Functions 1 and 2) occurs orders of magnitude faster than it takes for LHS Monte Carlo sampling to converge to a stable probability estimate. Though convergence with successive FE/LS Levels is relatively fast, non-monotonic convergence is observed, which is a generally observed trend in the convergence of numerical systems. In the usual case where it takes orders of magnitude more CPU time to run a simulation with the phenomenological model than to run a FE/LS response-surface code, the decoupled Monte Carlo FE/LS approach requires orders of magnitude less computer time overall than direct Monte Carlo analysis, with no appreciable loss of accuracy. Therefore, the many and varied tests applied here suggest that it is more efficient to expend computer-model FEVs on the building of the FE/LS response surface than to expend them in a direct Monte Carlo evaluation. Furthermore, the efficiency of the decoupled approach relative to the direct MC approach increases as the size of the computer model increases, and the convergence advantages seem to become more pronounced as the magnitude of the probability being resolved decreases. Both of these trends are very favorable indicators for the proposed FELSDMC method.

Finally, it would be instructive to substitute neural network and classical experimental-design response surfaces in the foregoing analyses to assess their efficiency and effectiveness versus FE/LS response surfaces, and also to compare the efficiency of non-Monte Carlo "reliability" approaches such as AMV (advanced mean value) and AMV+ [9]. Indeed, much of this work is currently being pursued by others under the same LDRD that funded this work.

REFERENCES

[1] Romero, V.J., "Efficient Propagation of Uncertainty and Probabilistic Behavior through Engineering Models via Decoupled Monte Carlo with Finite Element Response Surfaces Built from Structured Sampling," in preparation for submission to International Journal for Numerical Methods in Engineering

[2] Romero, V.J., "Noise and Bias vs. Model Resolution in Complex Physics Simulations and a Simple Response Surface Approach for Making Numerical Optimization More Affordable," submitted to Computer Modeling and Simulation in Engineering

[3] Eldred, M.S., Outka, Bohnhoff, W.J., Witkowski, W.P., Romero, V.J., Ponslet, E.J., and Chen, K.S., "Optimization of Complex Mechanics Simulations with Object-Oriented Software Design," in Computer Modeling and Simulation in Engineering, Vol. 1 No. 3, August, 1996, pp. 323-352.

[4] Iman, R.L., and Shortencarier, M.J., "A FORTRAN77 Program and User's Guide for the Generation of Latin Hypercube and Random Samples to Use with Computer Models," Sandia National Laboratories report SAND83-2365 (RG), printed March 1984.

[5] Wu, Y.-T., Millwater, H.R., and Cruse, T.A., "An Advanced Probabilistic Structural Analysis Method for Implicit Performance Functions", AIAA Journal J 17624, pp. 1-34.

[6] Wu, Y.-T., and Wirsching, P. H., "New Algorithm for Structural Reliability Estimation", ASCE Journal of Engineering Mechanics (Sept. 1987), vol. 113, no. 9, pp. 1319-1336.

[7] Patterson, T.N.L., "The Optimum Addition of Points to Quadrature Formulae," Math Comp. 22, 1968, pp. 847-856.

[8] Patterson, T.N.L., "On some Optimally and Lobatto based Quadrature Formulae," Math Comp. 22, 1968, pp. 877-881.

[9] Fossom, A.F., and Munson, D.E., "Probabilistic Creep Analysis of Underground Structures in Salt," J. Engineering Mechanics, Vol. 122, No. 3, March 1996, pp. 209-217.

Other Bibliography

Akin, J.E, *Application and Implementation of Finite Element Methods*, Academic Press, 1982

Bent, R.J., and Sethares, G.C., *FORTRAN[77] with Problem Solving: A Structured Approach*, Wadsworth, Inc., Belmont, CA., 1981.

Brebbia, C.A., Telles, J.C.F., and Wrobel, L.C., *Boundary Element Techniques - Theory and Applications in Engineering*, Springer-Verlag, 1984.

Ferziger, J. H., *Numerical Methods for Engineering Application*, John Wiley & Sons, 1981.

Hughes, T.J.R., *The Finite Element Method*, Prentice-Hall, 1987.

Strang, G., *Linear Algebra and Its Applications*, 2nd. Edition, Harcourt Brace Jovanovich, 1980.

TECPLOT User's Manual, Version 7, Amtec Engineering, Inc., Bellevue, Washington, 1996.

Zienkiewicz, O.C., *The Finite Element Method*, 3rd Edition., McGraw-Hill, 1977.

APPENDIX A: 2-D Rectalinear Coordinate Transform Relations

Here a procedure is described to obtain the coordinates of a Point **P** in one coordinate system given its coordinates in another system and the displacement, rotation, and scaling relationships between the two systems. Referring to the Figure A.1, rectangular coordinate System #1 has its origin at Point $\mathbf{O_1}$ and the right-handed orthogonal unit vector $\hat{i}$-$\hat{j}$ basis shown. The coordinates of **P** in this coordinate system are (x_P, y_P). Rectangular coordinate System #2 has its origin at Point $\mathbf{O_2}$ and the right-handed orthogonal unit vector $\hat{\xi}$ - $\hat{\eta}$ basis shown. The coordinates of **P** in this system are (ξ_P,η_P).

It is assumed that the origin of the translated coordinate system is known –*i.e.*, that the (x,y) coordinates of Point $\mathbf{O_2}$ are known. Then the vector $\vec{V}_{2-P}$ locating Point P from coordinate System #2 can be obtained by subtracting $\vec{V}_{1-2}$ from $\vec{V}_{1-P}$, where both are written in terms of x and y components. We have

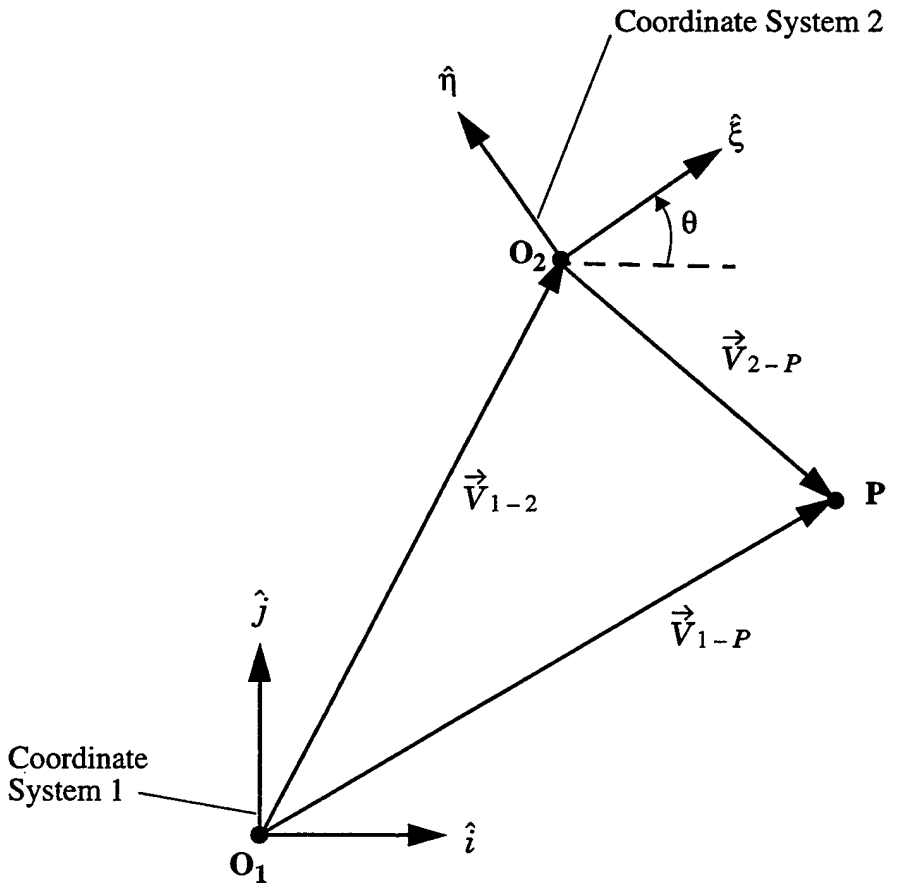

Figure A.1 Important quantities in locating Point **P** from two different coordinate systems.

$$\vec{V}_{1-P} = \vec{V}_{1-2} + \vec{V}_{2-P} \qquad \text{EQ A.1}$$

wherefrom

$$\vec{V}_{2-P} = \vec{V}_{1-P} - \vec{V}_{1-2} = (x_p - x_{O_2})\hat{i} + (y_p - y_{O_2})\hat{j}. \qquad \text{EQ A.2}$$

Alternatively in terms of System 2 quantities,

$$\vec{V}_{2-P} = S\xi_P\,\hat{\xi} + S\eta_P\,\hat{\eta} \qquad \text{EQ A.3}$$

where S is the scale factor for mapping physical distance between the two coordinate systems. The measure of physical distance in both coordinate systems is posed in terms of scalar factors x,y and ξ,η multiplying standard units of length, such as inches and centimeters, respectively. "This line is 1 inch long or 2.54 centimeters long." In the first case the length standard is inches, and there is 1.0 of them. In the second case the length standard is centimeters, and there are 2.54 of them. In mapping physical distances from one system of measure to another, the scale factor S compensates for the difference in the physical lengths of the standards of measure in the two systems:

(# of System 1 units) x (phys. length of Sys. 1 units) = (# of Sys. 2 units) x (phys. length of Sys. 2 units) EQ A.4

or, after rearranging,

$$\text{\# of System 1 units} = \text{\# of System 2 units} \times \frac{\text{phys. length of System 2 units}}{\text{phys. length of System 1 units}}. \qquad \text{EQ A.5}$$

The above ratio is the scale factor S under our conventions. If the standard unit of distance in System 2 is Z times the standard unit of distance in System 1, then the scale factor for mapping System 2 length multipliers ξ and η into System 1 multipliers x and y is $S = Z$.

Now we address the different rotational orientations in the two coordinate frames. Without loss of generality we consider the case where System 2 is rotated counterclockwise relative to System 1 through the angle θ as shown in the figure. Noting that the basis vectors are unit vectors, the projection of $\hat{\xi}$ along the x coordinate-direction is simply the cosine of the rotation angle θ, and the projection along y is the sine of the angle. We have:

$$\hat{i} \bullet \hat{\xi} = \cos\theta = x\text{-component of } \hat{\xi} \qquad \text{EQ A.6}$$

and

$$\hat{j} \bullet \hat{\xi} = \sin\theta = y\text{-component of } \hat{\xi} \qquad \text{EQ A.7}$$

whence

$$\hat{\xi} = \cos\theta\hat{i} + \sin\theta\hat{j}. \qquad \text{EQ A.8}$$

Analogously, we get

$$\hat{\eta} = -sin\theta\hat{i} + cos\theta\hat{j}. \qquad \text{EQ A.9}$$

Substituting EQ A.8 and EQ A.9 into EQ A.3 and equating to EQ A.2 yields a system of two simultaneous equations. Solving these together yields the final tranform relations between sets of coordinates in the two systems:

$$\xi_P = \frac{1}{S}[(x_p - x_{O_2})cos\theta + (y_p - y_{O_2})sin\theta] \qquad \text{EQ A.10}$$

$$\eta_P = \frac{1}{S}[-(x_p - x_{O_2})sin\theta + (y_p - y_{O_2})cos\theta]. \qquad \text{EQ A.11}$$

Various specializations of these are used in the program INTERP1C and are programmed in more efficient reduced forms where possible.

APPENDIX B: Selection of "Containing" Finite Element

As mentioned in Section 2.1.2, a selection algorithm in INTERP1C determines, for a specified Finite Element / Lattice Sampling response surface Level, which finite element contains the Point **P** where the interpolated value of the target function is desired. Figures B.2 and B.1 show the naming conventions and intrinsic coordinate systems (see Appendix C) of the various finite elements in Levels 1 - 6. Figures B.3 and B.4 show the flowchart logic used to determine which finite element contains **P** and the corresponding finite element subroutine to call for the particular element type. The logic for Levels 2, 4, and 6 is based on the 45-degree diagonally rotated global (x,y) coordinates shown in Figure 2.2. The logic for Levels 1, 3, and 5 is based on the unrotated global $(p1^*,p2^*)$ coordinates shown in Figure 2.2. Flowchart logic is not shown for Levels 1 and 3, where the entire parameter space is contained within one

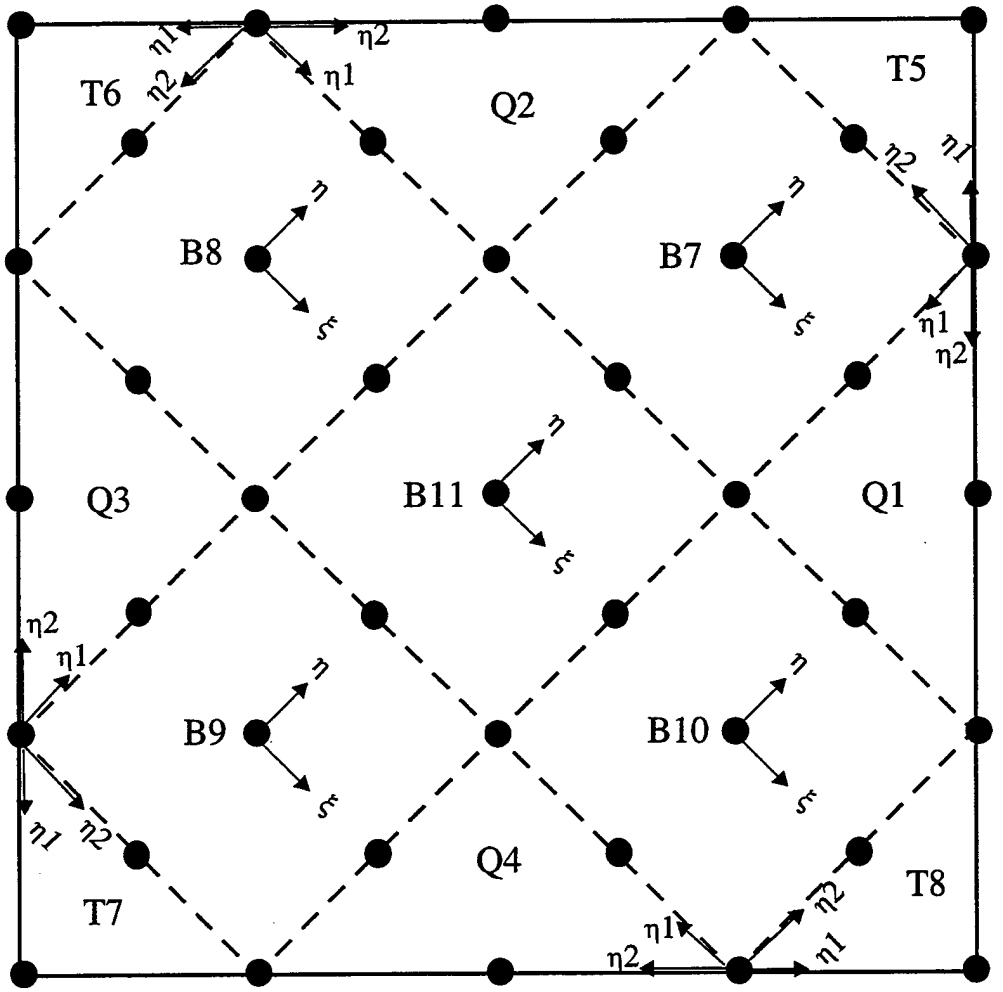

Figure B.1 Naming conventions and intrinsic coordinate systems of the various finite elements in Lattice Sampling Level 6.

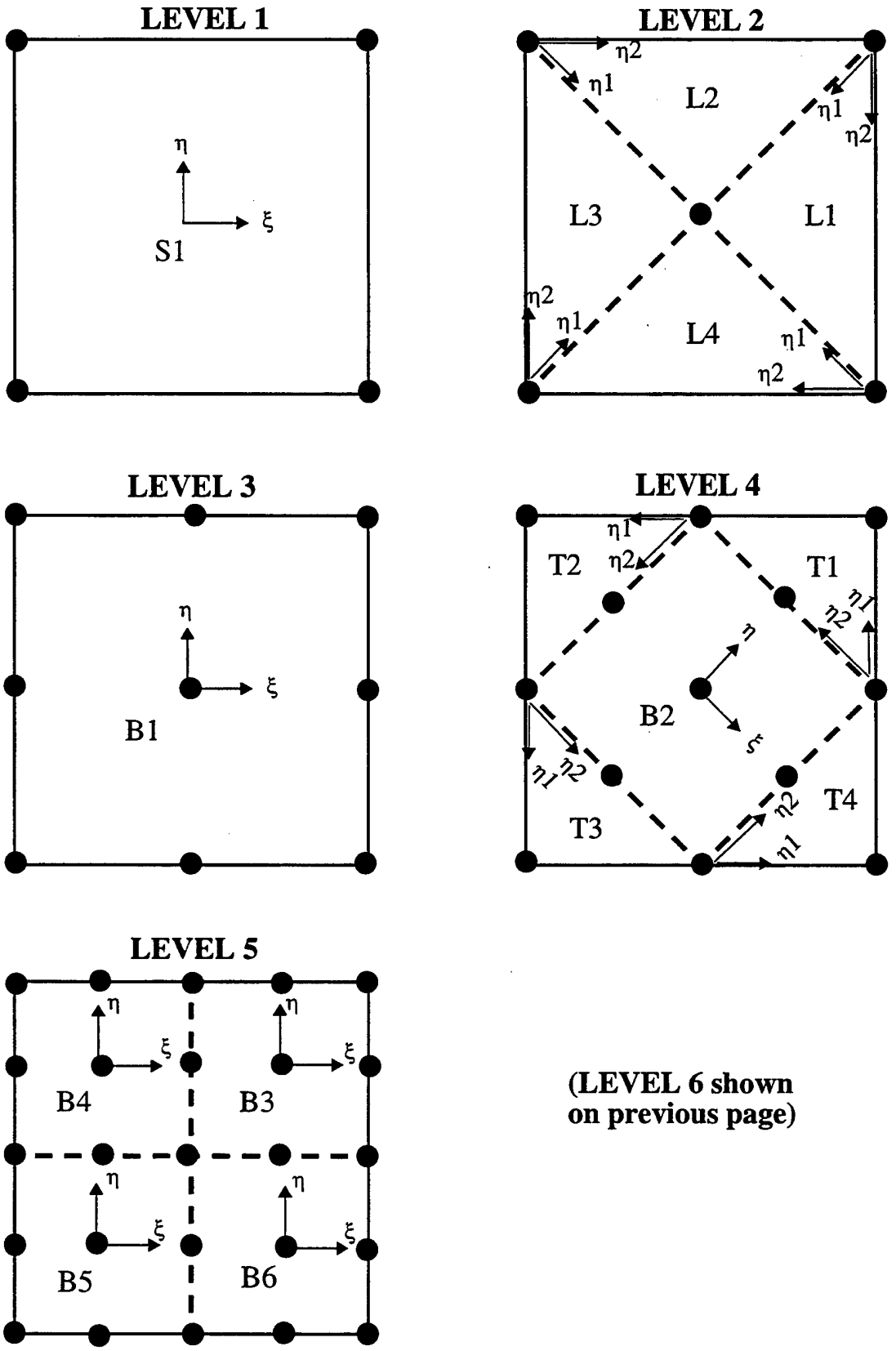

Figure B.2 Naming conventions and intrinsic coordinate systems of the various finite elements in Lattice Sampling Levels 1 - 5.

finite element, and the global ($p1^*$,$p2^*$) coordinates are identical to the local (ξ, η) intrinsic coordinates of the quad elements.

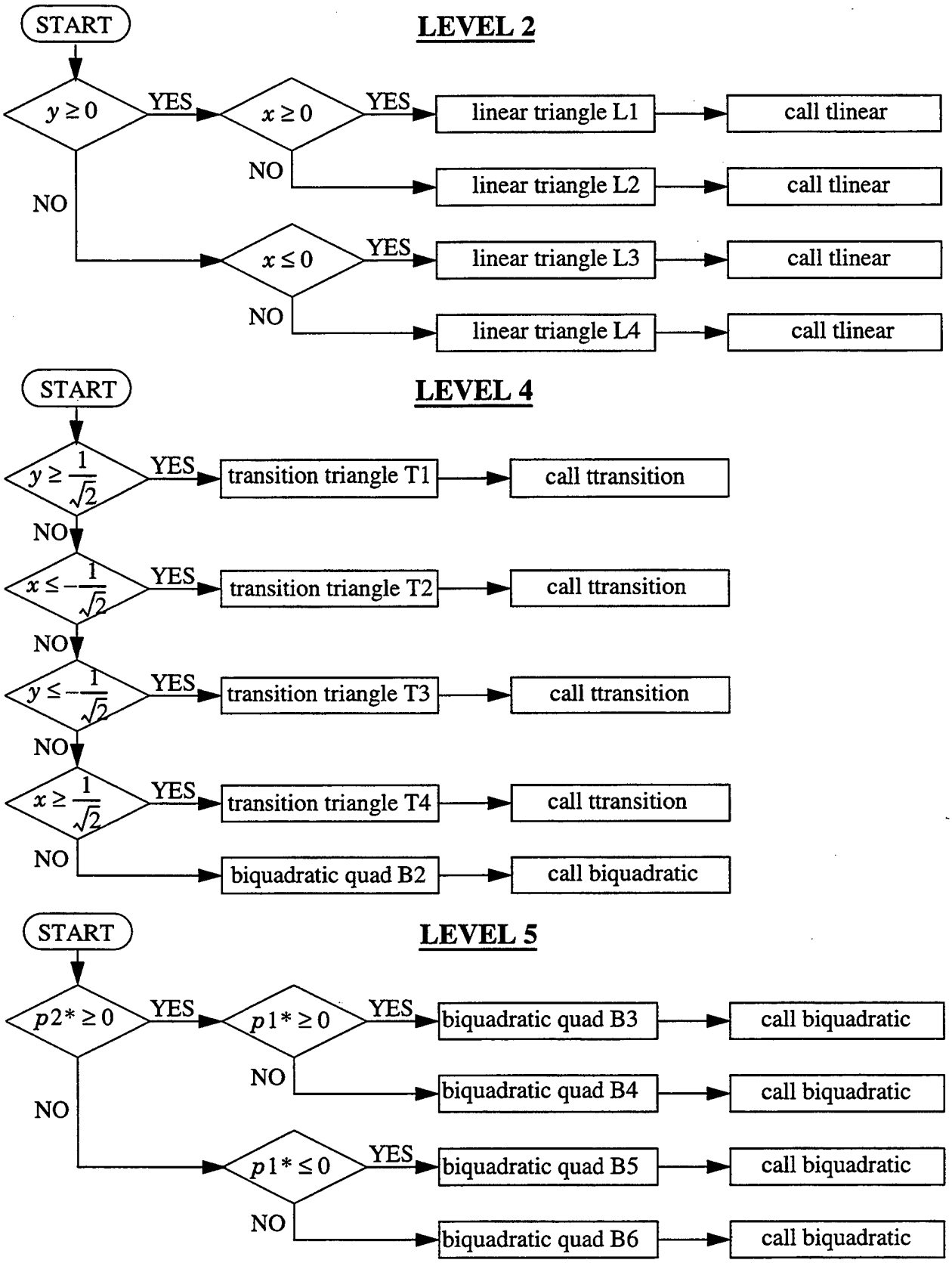

Figure B.3 Flowchart for "containing" element selection in INTERP1C for Levels 2, 4, 5.

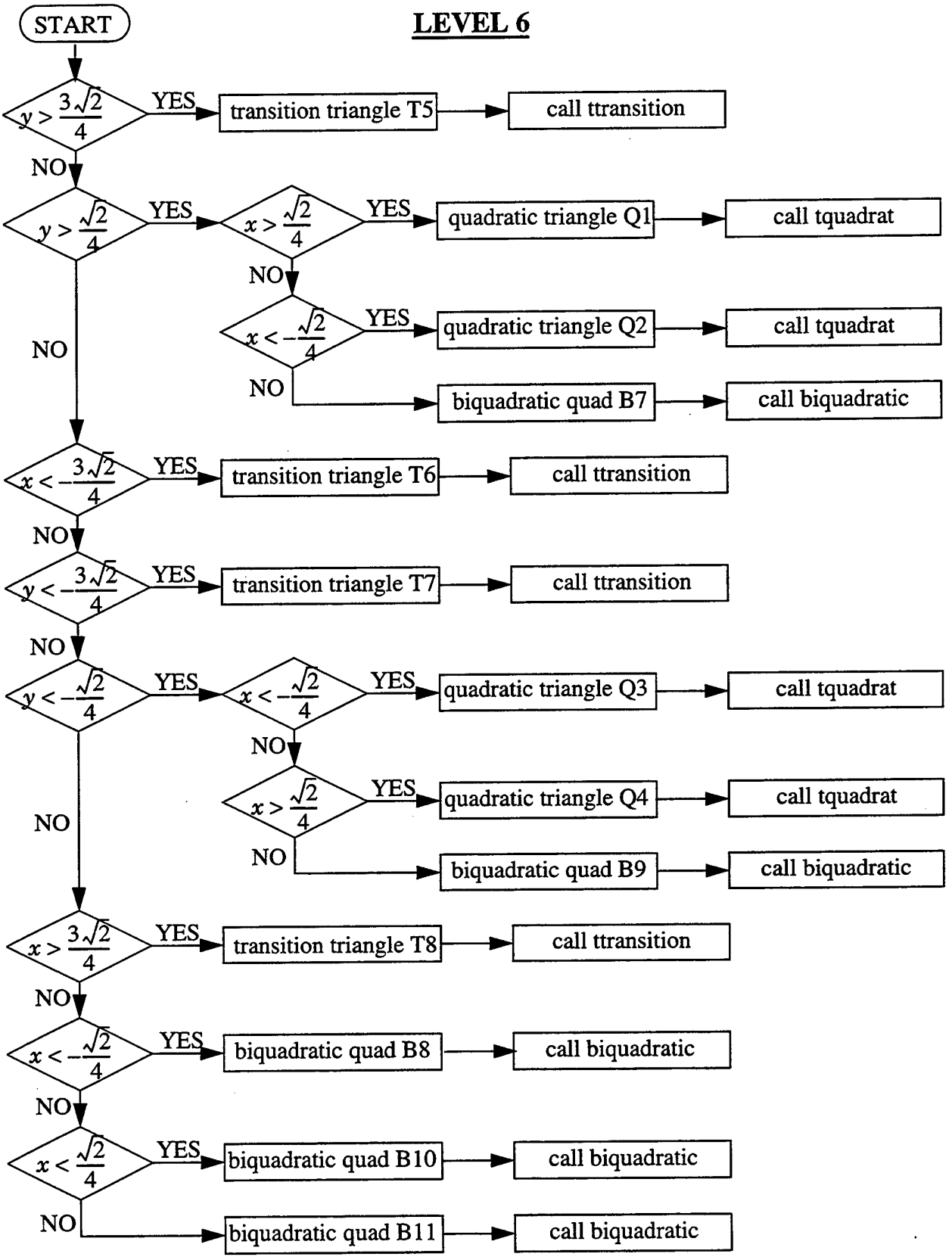

Figure B.4 Flowchart of the "containing" element selection logic in INTERP1C for Level 6.

APPENDIX C: Finite Element Formulations

As mentioned in Section 2.1.2, this appendix contains information regarding the intrinsic coordinate systems, local node numbering conventions, coordinate transform relations, and basis functions of the various types of finite elements used in Levels 1 - 6 of the Finite Element / Lattice Sampling methodology.

Triangular Elements

Intrinsic Coordinates and Transform Relations

The material presented here draws from the most convenient aspects of the developments in Brebbia *et al.*[1] and Zienkiewicz[2] for triangular finite elements.

The figure below shows a generic rectangular *u-v* coordinate system and a generic triangle with arbitrarily located vertices numbered in counterclockwise order. The coordinates of the vertices are shown, as those of a Point **P** lying within the triangle. A right-handed local $\eta 1$-$\eta 2$ coordinate system intrinsic to triangular finite elements of all types is also shown. The origin of the intrinsic coordinate system is at Vertex 3. Mneumonically, the $\eta 1$ coordinate points at Vertex 1 and the $\eta 2$ coordinate points at Vertex 2.

It is desired to determine the intrinsic $(\eta 1,\eta 2)$ coordinates of **P** given the global (u,v) coordinates of the three vertices and internal point **P**. The following coefficients are first computed.

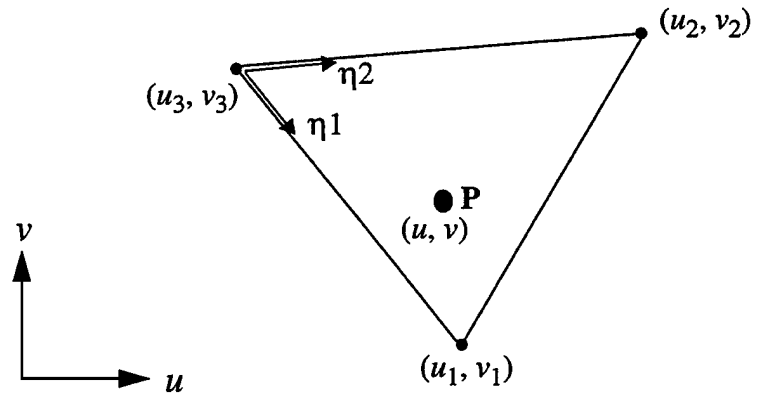

1. Brebbia, C.A., Telles, J.C.F., and Wrobel, L.C., *Boundary Element Techniques - Theory and Applications in Engineering*, Springer-Verlag, 1984.
2. Zienkiewicz, O.C., *The Finite Element Method*, 3rd Edition., McGraw-Hill, 1977.

$$a_1 = u_2 v_3 - u_3 v_2 \qquad \text{EQ 3}$$

$$a_2 = u_3 v_1 - u_1 v_3 \qquad \text{EQ 4}$$

$$b_1 = v_2 - v_3 \qquad \text{EQ 5}$$

$$b_2 = v_3 - v_1 \qquad \text{EQ 6}$$

$$c_1 = u_3 - u_2 \qquad \text{EQ 7}$$

$$c_2 = u_1 - u_3 \qquad \text{EQ 8}$$

For programming purposes, these coefficients can be written in the general form

$$a_i = u_j v_k - u_k v_j \qquad \text{EQ 9}$$

$$b_i = v_j - v_k \qquad \text{EQ 10}$$

$$c_i = u_k - u_j \qquad \text{EQ 11}$$

with the following cyclic permutations of the indices for the specific cases.

i	j	k
1	2	3
2	3	1

The intrinsic coordinates of Point **P** can then be found from its original (u_P, v_P) coordinates in the global frame by

$$\eta 1 = \frac{1}{2A}(a_1 + b_1 u + c_1 v) \qquad \text{EQ 12}$$

$$\eta 2 = \frac{1}{2A}(a_2 + b_2 u + c_2 v) \qquad \text{EQ 13}$$

where 2A is twice the area of the triangle. By the rule of determinants[3],

$$2A = b_1 c_2 - b_2 c_1 . \qquad \text{EQ 14}$$

The following equation yields the dependent parameter $\eta 3$, which is a convenient third variable that can be used in the triangular finite element shape functions presented next.

$$\eta 3 = 1 - \eta 1 - \eta 2 \qquad \text{EQ 15}$$

---

3. Strang, G., *Linear Algebra and Its Applications*, 2nd. Edition, Harcourt Brace Jovanovich, 1980.

Note that $\eta 1 = 1$ at Vertex 1, and $\eta 1 = 0$ at the other two vertices, and analogously for the other two triangular shape-function parameters $\eta 2$ and $\eta 3$. Also, at any point on or inside the triangle, the three parameters sum to unity (by definition, *cf.* EQ 12).

Linear Triangles

Linear Triangle finite elements have a node at each vertex as shown, and appear in FE/LS Level 2 only. The values of the target function at each node point, ϕ_i, are presumed

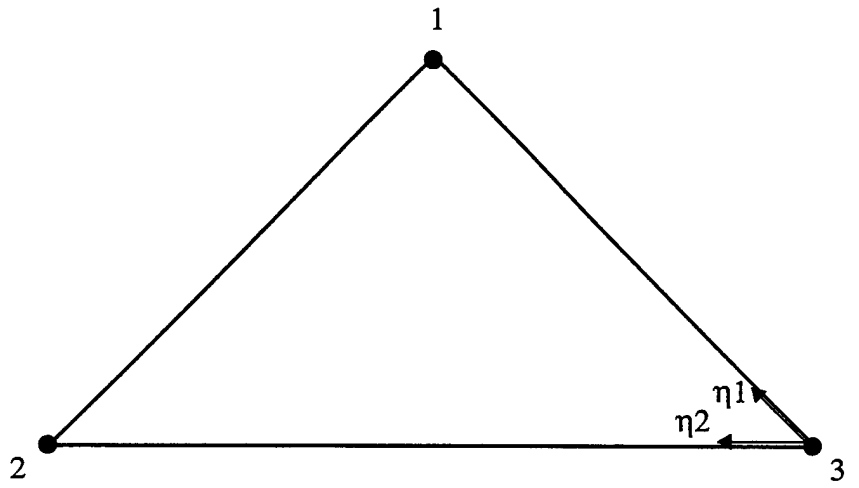

known, wherefrom the interpolated value at the point **P** within the triangle is determined as

$$\phi(u, v) = \sum_{i=1}^{3} \phi_i N_i(u, v), \qquad \text{EQ 16}$$

and the Linear Triangle finite element basis or "shape" functions N_i are given by

$$N_1 = \eta 1 \qquad \text{EQ 17}$$

$$N_2 = \eta 2 \qquad \text{EQ 18}$$

$$N_3 = \eta 3. \qquad \text{EQ 19}$$

These shape functions, and those defined subsequently for other types of finite elements, act as weighting functions that weight the contributions of the various nodal values ϕ_i according to the proximity of the nodes to the point **P**, closer nodes having a stronger contribution than further ones. Sets of finite element shape functions have the properties that they sum to 1.0 at any point on or within the element, and each has a value of zero at every node except the node it is numbered after and associated with (for which the nodal value is unity). Thus, when the point **P** lies on a node, the only contribution to the interpolated value at **P** comes from the node that **P** lies on, and the interpolated value is identically the nodal value there.

Letting the point **P** assume arbitrary global coordinates (u,v), it can be shown by substituting EQs 3-8, 12-15, and 17-19 into EQ 16 and factoring, that the form of the interpolation function $\phi(u,v)$ is $C_1 + C_2u + C_3v$, a complete bilinear polynomial in the global coordinates (where the C_i are constants).

Quadratic-to-Linear Transition Triangles

Transition Triangles appearing in FE/LS Levels 4 and 5 have four nodes at which the value of the target function must be calculated. The vertices of the triangular element are numbered in the same manner as for the linear triangle, with the fourth node being midway between Vertices 2 and 3. These elements transition from quadratic behavior of the response

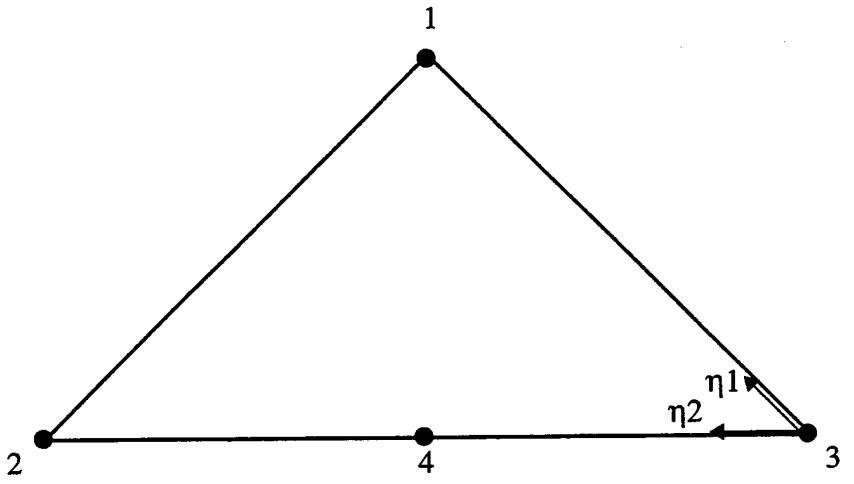

surface along the edge defined by Nodes 2 and 3 to linear variation over the other two edges of the element. The interpolated value at the point **P** within the triangle is determined as the superposition of nodal values and finite element basis functions as in EQ 16, where the particular basis functions for this element are

$$N_1 = \eta_1 \qquad \text{EQ 20}$$

$$N_2 = \eta_2(1 - 2\eta_3) \qquad \text{EQ 21}$$

$$N_3 = \eta_3(1 - 2\eta_2) \qquad \text{EQ 22}$$

$$N_3 = 4\eta_2\eta_3. \qquad \text{EQ 23}$$

These shape functions were derived from the procedure outlined in Akin[4] for enriching shape functions to produce transition and other special finite elements.

Quadratic Triangles

Quadratic Triangles have six nodes and appear in Level 6 only. The vertices are labeled in the same manner as for linear triangles, and the mid-side nodes are labeled in similar coun-

4. Akin, J.E, *Application and Implementation of Finite Element Methods*, Academic Press, 1982.

terclockwise fashion as shown. Note that Node #4 is on a different edge (*i.e.*, between different pairs of vertices) for this triangle versus the linear-to-quadratic transition triangle.

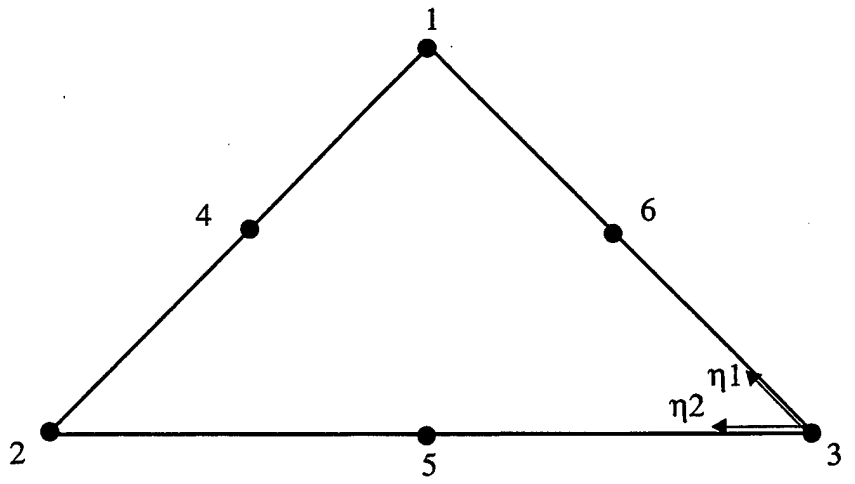

The interpolated value at the point **P** within the triangle is determined as the superposition of nodal values and finite element basis functions as in EQ 16, where the particular basis functions for this element are:

$$N_1 = \eta_1(2\eta_1 - 1) \qquad \text{EQ 24}$$

$$N_2 = \eta_2(2\eta_2 - 1) \qquad \text{EQ 25}$$

$$N_3 = \eta_3(2\eta_3 - 1) \qquad \text{EQ 26}$$

$$N_4 = 4\eta_1\eta_2 \qquad \text{EQ 27}$$

$$N_5 = 4\eta_2\eta_3 \qquad \text{EQ 28}$$

$$N_6 = 4\eta_3\eta_1. \qquad \text{EQ 29}$$

It can be shown that the form of the interpolation function $\phi(u, v)$ is $C_1 + C_2u + C_3v + C_4uv + C_5u^2 + C_6v^2$, a complete biquadratic polynomial in the global coordinates.

Square Elements

Intrinsic Coordinates

The intrinsic coordinates for the types of rectangular finite elements used in this work are orthogonal right-handed ξ-η systems with origin at the center of the elements as shown in the following figures. The coordinate systems are oriented along vertical and horizontal directions, as are the respective sides of the square elements. The coordinates range from -1 to 1 in each direction. The methodology for transforming the coordinates of some point **P** within the element from global to local (ξ,η) coordinates is described in Appendix A.

1-D Lagrange Polynomials

The shape functions for our 2-D square finite elements can be written as products of 1-D Lagrange polynomials. The general formulas for these over a domain ranging from -1 to 1 are, in terms of the generic length coordinate γ measured positive to the right from the mid-point of the domain,

LINEAR:

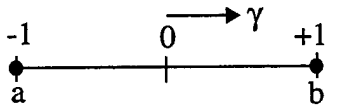

$$l_a(\gamma) = \frac{1-\gamma}{2} \qquad \text{EQ 30}$$

$$l_b(\gamma) = \frac{1+\gamma}{2} \qquad \text{EQ 31}$$

QUADRATIC:

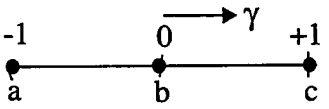

$$q_a(\gamma) = \frac{\gamma(\gamma-1)}{2} \qquad \text{EQ 32}$$

$$q_b(\gamma) = 1-\gamma^2 \qquad \text{EQ 33}$$

$$q_c(\gamma) = \frac{\gamma(\gamma+1)}{2}. \qquad \text{EQ 34}$$

Linear Square

Linear Square finite elements have a node at each corner, and appear in Level 1 only. Nodes are numbered to reflect the product-rule model in Hughes[5] (illustrated in the following figure) for writing 2-D quadratic element shape functions as products of 1-D Lagrange polynomials in each coordinate direction[6]. Taking Node 1, the lower-left node in the square element as an example, its shape function is the product of Lagrange polynomials associated with the lower and left nodes of the 1-D elements in the figure. Similar considerations yield shape functions 2, 3, and 4, respectively, at the lower-right, upper-left, and upper-right nodes of the element. The resulting shape functions are

$$N_1(\xi,\eta) = l_a(\xi)l_a(\eta) \quad (=(1-\xi)(1-\eta)/4) \qquad \text{EQ 35}$$

$$N_2(\xi,\eta) = l_b(\xi)l_a(\eta) \qquad \text{EQ 36}$$

---

5. Hughes, T.J.R., *The Finite Element Method*, Prentice-Hall, 1987.
6. The product-rule analogy works for arbitrary-dimensional finite elements, which would be used in representing response-surfaces for N-dimensional optimization and nondeterministic problems.

$$N_3(\xi,\eta) = l_a(\xi)l_b(\eta) \qquad \text{EQ 37}$$

$$N_4(\xi,\eta) = l_b(\xi)l_b(\eta) \qquad \text{EQ 38}$$

As usual, the interpolated value at a point within the element is determined by the superposition of nodal values and these finite element basis functions in analogy with EQ 16. It can be shown that the form of the resulting interpolation function $\phi(u,v)$ is $C_1 + C_2u + C_3v + C_4uv$, a complete bilinear polynomial in the global coordinates.

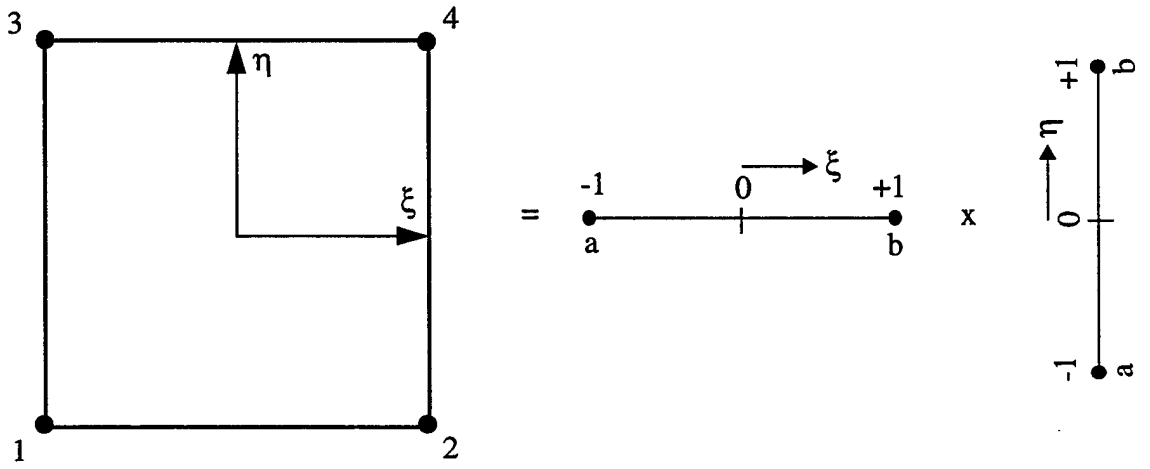

(Illustration of Hughes' product rule analogy for generation of 2-D shape functions from 1-D Lagrange polynomials in each coordinate direction.)

Biquadratic Square

Biquadratic Squares have nine regularly spaced nodes as shown in the figure below, and appear in Finite Element / Lattice Sampling Levels 3, 4, 5, and 6. Nodes are numbered for the product rule with quadratic Lagrange polynomials. The resulting shape functions are

$$N_1(\xi,\eta) = q_a(\xi)q_a(\eta) \qquad \text{EQ 39}$$

$$N_2(\xi,\eta) = q_b(\xi)q_a(\eta) \qquad \text{EQ 40}$$

$$N_3(\xi,\eta) = q_c(\xi)q_a(\eta) \qquad \text{EQ 41}$$

$$N_4(\xi,\eta) = q_a(\xi)q_b(\eta) \qquad \text{EQ 42}$$

$$N_5(\xi,\eta) = q_b(\xi)q_b(\eta) \qquad \text{EQ 43}$$

$$N_6(\xi,\eta) = q_c(\xi)q_b(\eta) \qquad \text{EQ 44}$$

$$N_7(\xi,\eta) = q_a(\xi)q_c(\eta) \qquad \text{EQ 45}$$

$$N_8(\xi,\eta) = q_b(\xi)q_c(\eta) \qquad \text{EQ 46}$$

$$N_9(\xi,\eta) = q_c(\xi)q_c(\eta) \qquad \text{EQ 47}$$

Again, the interpolated value at a point within the element is determined by the superposition of nodal values and these finite element basis functions in analogy with EQ 16. It can be shown that the form of the resulting interpolation function $\phi(u,v)$ is $C_1 + C_2u + C_3v + C_4uv + C_5u^2 + C_6v^2 + C_7u^2v + C_8uv^2 + C_9u^2v^2$, a complete biquadratic polynomial in the global coordinates with several auxiliary higher-order degrees of freedom.

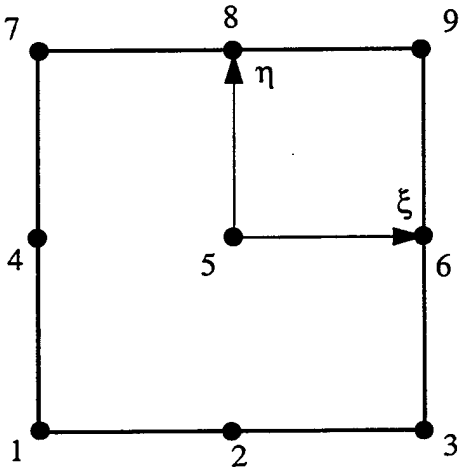

Distribution:

4 Susan D. Bankston
c/o Mechanical Engineering Dept.,
Texas A&M University
College Station, Texas 77844

1	MS0769	5800	D. S. Miyoshi
1	MS0747	6412	G. D. Wyss
1	MS0405	6413	A. S. Benjamin
1	MS0746	6411	L. A. Painton-Swiler
1	MS0746	6411	D. G. Robinson
1	MS0841	9100	P. J. Hommert
1	MS0828	9101	T. C. Bickel, route to 9102, 9103, 9104
1	MS0836	9111	W. H. Hermina, route to 9114, 9115
1	MS0834	9112	A. C. Ratzel, route to 9116, 9117/9118
1	MS0835	9113	S. N. Kempka
1	MS0835	9113	B. F. Blackwell
20	MS0835	9113	V. J. Romero
1	MS0835	9113	Day File
1	MS0819	9231	T. G. Trucano
1	MS0439	9234	D. R. Martinez
1	MS0439	9234	J. R. Red-Horse
1	MS0439	9234	M. S. Eldred
1	MS0557	9741	T. L. Paez
1	MS0829	12323	K. V. Diegert
1	MS0405	12333	D. D. Carlson
1	MS0405	12333	M. P. Bohn
1	MS0405	12333	T. R. Jones
1	MS9018	8940-2	Central Technical Files
2	MS0899	4916	Technical Library
2	MS0619	12690	Review & Approval for DOE/OSTI

TOTAL COPIES = 50

Report Number (14) SAND--98-0567

Publ. Date (11) 199803

Sponsor Code (18) DOE/DP, XF

UC Category (19) UC-705, DOE/ER

DOE